HHS Public Access

Author manuscript

Bioorg Med Chem. Author manuscript; available in PMC 2016 July 01.

Published in final edited form as:

Bioorg Med Chem. 2015 July 1; 23(13): 3603–3617. doi:10.1016/j.bmc.2015.04.006.

Effect of chirality on cellular uptake, imaging and photodynamic therapy of photosensitizers derived from chlorophyll-a

Avinash Srivatsan[a], **Paula Pera**[a], **Penny Joshi**[a], **Yanfang Wang**[a], **Joseph R. Missert**[a], **Erin C. Tracy**[b], **Walter A. Tabaczynski**[a], **Rutao Yao**[c], **Munawwar Sajjad**[c], **Heinz Baumann**[b,*], and **Ravindra K. Pandey**[a,*]

[a]Photodynamic Therapy Center, Cell Stress Biology, Roswell Park Cancer Institute (RPCI), Buffalo, NY 14263

[b]Department of Molecular and Cellular Biology, Roswell Park Cancer Institute (RPCI), Buffalo, NY 14263

[c]Department of Nuclear Medicine, SUNY, Buffalo, NY 14221

Abstract

We have previously shown that the ^{124}I-analog of methyl 3-(1'-*m*-iodobenzyloxy) ethyl-3-devinyl-pyropheophorbide-a derived as racemic mixture from chlorophyll-a can be used for PET (positron emission tomography) -imaging in animal tumor models. On the other hand, as a non-radioactive analog, it showed excellent fluorescence and photodynamic therapy (PDT) efficacy. Thus, a single agent in a mixture of radioactive (^{124}I-) and non-radioactive (^{127}I) material can be used for both dual-imaging and PDT of cancer. Before advancing to Phase I human clinical trials, we evaluated the activity of the individual isomers as well as the impact of a chiral center at position-3[1] in directing *in vitro/in vivo* cellular uptake, intracellular localization, epithelial tumor cell-specific retention, fluorescence/PET imaging, and photosensitizing ability. The results indicate that both isomers (racemates), either as methyl ester or carboxylic acid, were equally effective. However, the methyl ester analogs, due to subcellular deposition into vesicular structures, were preferentially retained. All derivatives containing carboxylic acid at the position-17[2] were noted to be substrate for the ABCG2 (a member of the ATP binding cassette transporters) protein explaining their low retention in lung tumor cells expressing this transporter. The compounds in which the chirality at position-3 has been substituted by a non-chiral functionality showed reduced cellular uptake, retention and lower PDT efficacy in mice bearing murine Colon26 tumors.

Graphical Abstract

Corresponding authors: Heinz.Baumann@roswellpark.org (Heinz Baumann), Ravindra.pandey@roswellpark.org (Ravindra K. Pandey).

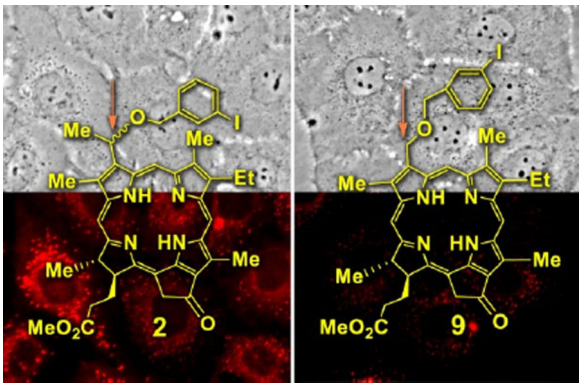

1. Introduction

Over the last decade, the field of chirality has witnessed revolutionary changes with increased emphasis placed on pharmacology, pharmacokinetics and pharmacodynamics of enantiomers representing biologically active compounds[1]. Indeed, there are numerous examples in the literature, which confirm the benefits of recognizing chirality in a drug entity and its relationship to bioactivity[2,3]. Therefore, it is important not to ignore chirality of molecules considered for drug development. Although not yet specifically demanded, it appears to be prudent to evaluate at the onset of the drug development process the pharmacologic, pharmacokinetic, pharmacodynamic, and toxicology profiles of the racemate and the individual *enantiomers to justify the development of a specific form of the chiral drug for human use. The* Food and Drug Administration (FDA) has stringent guidelines with respect to the approval of a compound containing a mixture of stereo- and diastereoisomers for human clinical trials. Hence, the stability, tumor uptake and biological efficacy (including the toxicity) of the individual isomer should be determined before initiating Phase I human clinical trials. There are several examples in the literature where *R*- and *S*-isomers show a significant difference in biological activity and toxicity. For example, *S*-Warfarin is 6–fold more effective than *R*-Warfarin[4]. *R*-Thalidomide[5] is an inactive compound which converts to *S*-Thalidomide and causes deformities in infants.

The concept of stereoselectivity in drug action, transport and elimination has been well characterized for a select number of investigated endogenous and exogenous chemicals[6–8]. The stereoselectivity also seems to play an important in pharmacological or physiological properties of drug candidates[9,10]. There are several examples in which a chiral drug has a desirable, but different therapeutic effect for both isomers. For example, quinidine is an antiarrythmic, whereas quinine is an antimalarial. Similarly a synthetic drug propoxyphene: the dextropropoxyphene is an analgesic agent, whereas levoprophoxyphene is devoid of analgesic properties but it is an effective antitussive[11].

It has also been shown that some enantiomers exhibit therapeutic advantages. For example in indacrinone (diuretic), the *R*-isomer is the active diuretic, the corresponding corresponding S-isomer acts as an uricosuric, promoting uric acid secretion and, therefore, antagonizing the undesired side-effect of the *R*-isomer. It provides a good argument for

marketing indacrinone as an isomeric mixture. Studies have shown that *R:S* mixture of 9:1 ratio affords an optimal therapeutic effect[12].

The stereoisomers composition of drug substance is rapidly becoming an important issue in the development, and clinical use of pharmaceutical preparations, and health organization authorities, e. g. United States Food and Drug Administration (FDA) currently adopt a strict policy to develop drugs only in their single stereoisomer form if the data justify marketing a single enantiomer to ensure optimal efficacy and avoid unwanted side-effects[13]. Among benzoporphyrin derivatives, the ring-A and ring-B Diels-Alder products obtained by reacting protoporphyrin IX with dimethylacetyledicarboxylate, the ring-A adduct as a monocarboxylic acid showed better efficacy in treating age related macular degeneration (AMD) by PDT than the corresponding ring-B isomer[14]. In an animal study, the same adduct also produced enhanced efficacy over the other isomer in treating tumor by PDT[15].

In our initial attempts to develop more effective photodynamic therapy agents than Photofrin™ with reduced skin phototoxicity, we synthesized a series of alkyl ether analogs of pyropheophorbide-a introduced at various peripheral positions of the tetrapyrrolic structure[16–18]. A detailed biological evaluation of these compounds indicated that besides overall lipophilicity, the position of the alkyl ether group in the molecule made a remarkable difference in tumor uptake and long-term photodynamic therapy (PDT) efficacy. The structure activity relationship (SAR) studies[19,20] have been extremely useful in selecting improved PDT agents in porphyrin[21], porphycene[22], texaphyrin (expanded ring system)[23], phthalocyanines[24] and naphthalocyanine systems[25].

To develop a multifunctional agent for cancer imaging and therapy, we have shown that the 3-[1’-(*m*-iodobenzyloxy)ethyl]-3-devinylpyro pheophorbide-a derived from chlorophyll-a can be used for fluorescence image-guided photodynamic therapy (PDT) of cancer[26–29]. Interestingly, the corresponding ^{124}I-radiolabeled analog obtained by replacing the iodo-group with radioactive iodine showed excellent tumor-imaging ability by positron nuclear tomography (PET)[30–32]. The combination of dual-function agent (fluorescence and PET) provides advantages over the single imaging technique[33]. For example, fluorescence imaging offers a cost effective way to accomplish image-guided therapy, but has limitations in quantification of tissue-localized drug and in imaging deeply seated tumors. In contrast, PET is capable of quantitative whole body imaging, but is much more expensive for image-guided therapy. Thus, PET and fluorescence imaging could complement each other[34].

The toxicity of ^{124}I-labeled and non-labeled compounds at variable doses was also investigated in mice and rats following the US FDA requirements and no significant normal organ toxicity was observed by histopathologic analyses[35]. The treatments of various cell types in tissue cultures with 3-[1’-(*m*-iodobenzyloxyethyl)-3-devinylpyropheophorbide-a and structural analogs[36] have indicated that side groups added to the porphyrin ring affect the mode of cellular uptake and intracellular distribution. Not yet known is the impact of stereoisomerism on the cell biology of the compounds. The objectives of the present study was (i) to elucidate the biological properties of the individual stereoisomers, and the importance of a chiral center present at position-3 of methyl 3-[1’-(*m*-iodobenzyloxyethyl)-3-devinyl pyropheophorbide-a and the corresponding carboxylic acid

derivative, and (ii) to investigate if there is any correlation between the biological efficacy of individual isomers, and the importance of the presence of the chiral center at position 3[1].

For the synthesis of the desired analogs (Scheme 1), the vinyl-group present at position-3 of methyl pyropheophorbide-a **1** was replaced with a (1'-*m*-iodobenzyloxy)ethyl substituent. The resulting product **2** was isolated as a mixture of isomers, and then separated into individual isomers **3** and **4**. To investigate the importance of chirality at position-3, a 3-(*m*-1'-iodobenzyloxy)methyl group was introduced into methyl pyropheophorbide-a **1** yielding compound **9**. These compounds were comparatively analyzed for cellular uptake, intracellular localization, fluorescence imaging and PDT efficacy using a panel of informative human and murine cancer cell systems. The results indicated that while the isolated isomeric compounds yielded identical activity as the corresponding diasteromeric mixtures, there were striking differences in cell type-specific retention and, thus, PDT efficacies, as function of the compounds' chirality and charge. The findings are discussed in view of further development of 3-[1'-(*m*-iodobenzyloxyethyl)-3-devinylpyro pheophorbide-a as tumor-specific theranostics.

2. Results and discussion

2.1. Synthesis and Characterization

Methyl 3-[1'-(*m*-iodobenzyloxy) ethyl] pyropheophorbide-a **2** was synthesized from methyl pyropheophorbide-a **1** (Scheme 1), which was extracted from *Spirulina pacifica* by following known methodologies[37,38].

Compound **2**, isolated as a diasteromeric mixture, was separated into individual isomers **3** and **4** by HPLC with retention times 5.9 min and 6.7 min, respectively (Fig. 1). The tentative configuration was assigned on the basis of literature report[39]. Purity of the individual isomers was also confirmed by co-injecting the individual isomer in combination with the isomeric mixture of the starting material **2** (see supporting material).

Previous characterization of structurally related pyropheophorbide-a derivatives has indicated that an acidic charge introduced at the position-17[2] prominently altered cellular uptake, subcellular localization and PDT efficacy[40]. To determine whether the effect was also achieved with compound **2** and its separated isomers **3** and **4**, these compounds, bearing methyl ester functionality, were hydrolyzed with aqueous lithium hydroxide (LiOH). The products, containing the corresponding carboxylic acid side groups, represent compounds **2a, 5** and **6**, respectively, and were evaluated in a comparative manner. To determine the influence of the chiral center at position-3 (IUPAC nomenclature) in compound **2**, compound **9** was synthesized by following the approach depicted in Scheme 1. In brief, the methyl pyropheo-phorbide-a **1** was reacted with osmium tetroxide (OsO_4) and sodium periodate ($NaIO_4$). The 3-formyl derivative **7**, obtained in 90% yield, was reacted with sodium borohydride ($NaBH_4$), and he 3-hydroxymethyl derivative **8** was obtained in quantitative yield. The reaction of **8** with HBr/AcOH and then with *m*-iodobenzylalcohol produced the hexyl ether derivative **9** in high yield

The structures of all compounds were confirmed by NMR (^{1}H and ^{13}C) and mass spectrometry. ^{1}H NMR spectra of compounds **2, 3, 4**, and **9** (Fig. 2 and supporting material, Figs. S2, S3 and S8) illustrate the spectral differences observed for the two isomers. In compound **2** (the isomeric mixture of **3** and **4**) most resonances of the individual isomers overlap. However, a few protons show slight differences in chemical shift between the two stereoisomers. This is illustrated in Fig. 2, where the 3^{1} methyl proton doublet appears at 2.17 ppm for the *R*- form **3** and 2.16 ppm for the *S*-form **4**. The mixture in compound **2** shows both doublets. Further differences in the two forms are observed for $H3^{3}$, the 18^{1} methyl protons, and two of the ring methyl groups. In contrast, the NMR spectrum of compound **9**, which lacks chirality at position-3, displays only a single set of resonances for each proton. Other major differences observed between **9** and the chiral compounds (**3** or **4**) are as follows: In **9**, the 3^{1} methyl and methine proton signals are absent. Instead, a singlet due to $–CH_2$-O-R, integrating for two protons at 5.72 ppm is observed. Also, the non-equivalence of the benzylic protons is lost, and a somewhat deshielded singlet integrating for two protons is observed at 4.74 ppm. None of the compounds show any significant difference in absorption and fluorescence properties. In both compounds **2** and **9**, excitation of the absorption bands at 660 nm (CH_2Cl_2) produces fluorescence at 675 (strong) and 720 nm (weak) respectively

2.2. Both stereoisomers 3 and 4 show similar biological properties in vitro

Since uptake and subcellular distribution of pyropheophorbides are subject to cell type-specific difference[36] the isolated isomers, as well as the isomeric mixture, were tested in representative cultures of fibroblastic and epithelial cells. The initial survey determined *in vitro* uptake, intra-cellular localization and *in vitro* PDT efficacy in murine Colon26 cells (supporting material information: Fig. S19). These cells were selected because they also permitted a subsequent comparison of the compounds *in vivo* by growing Colon26 tumor in isogeneic BALB/c mice. The key findings made with the murine cells were then verified in primary cultures of cells generated from surgical specimens obtained from lung cancer cases treated at RPCI.

Uptake and subcellular localization in Colon26 cells was quantified by flow cytometry using an Image Stream instrument (Fig. 3). As shown in Fig. 3A, the cellular accumulation of isolated isomers **3** and **4** over a 24-hour period is comparable and does not significantly differ from that of the mixture of isomers present in compound **2**. In contrast, the isomers **5** and **6** of the carboxylic acid derivative, like the mixture of isomers in compound **2a**, reach approximately 2-fold higher level. The image analysis of individual cells (Fig. 3B) indicates that the isomers **3** and **4**, like the compound **2**, are present in subcellular compartments largely not congruent with either mitochondria or lysosomes/endosomes (Fig. 3C). The carboxylic acid derivatives, however, show co-distribution with the mitochondrial marker (Fig. 3B & **C**).

The flow cytometric analysis of the compounds' cellular distribution involves imaging of suspended cells. While this permits a precise measurement of cell-associated compounds, it does not provide an accurate definition of the subcellular distribution applicable to matrix-adherent cells. Moreover, considering that the uptake as well as retention of the compounds

can substantially differ among cell type, including those intended to be the therapeutic targets, the comparison of the isomer's uptake was extended to primary cultures of stromal fibroblasts and epithelial cells derived from human lung tumor tissue. The analyses of the cellular uptake relied on microscopic imaging of the live adherent cells. The large size of the cells facilitated a visualization of the subcellular distribution at higher resolution than achieved by image stream analysis.

In the example of tumor stromal fibroblasts, uptake of the isolated isomers **3–6** was monitored at three stages (Fig. 4). The first stage determines the level of cell surface binding versus diffusion into the cells during a 30-min incubation of the cells on ice (prevention of endocytotic processes). The second stage determines internalization and intracellular deposition of the compounds after an 4-hour incubation at 37°C in full culture medium containing compound. Finally, the third stage determines cellular retention of the compounds after 4–24 hours incubation (or chase) in compound-free culture medium. The fluorescent microscopic images of the compounds' distribution indicate the following features: (i) both the methyl ester (compounds **3** and **4**) and carboxylic acid derivatives (compounds **5** and **6**) do not show appreciable binding to cell surface; (ii) internalization by diffusion into the ER and mitochondrial compartments is evident already in cultures treated on ice; (iii) during incubation at 37°C, the uptake of compounds increases, with a major portion of the methyl ester derivatives deposited into subcellular, optically dense granular structures, whereas, the carboxylic acid derivatives remain primarily associated with ER/mitochondria; (iv) based on quantitative measurements of fluorescence (data not shown), the uptake of the carboxylic acid derivatives over a 4-hour culture period exceeds 4–5-fold that of the methyl ester derivatives; (v) the methyl ester derivatives are retained by the cells with an apparent half-life of approximately 12–24 hours whereas the carboxylic acid derivatives are lost from the cells at a faster rate resulting in an apparent half-life of 2–4 hours; and (vi), there is no appreciable difference between the two isomeric compounds **3** and **4** and between the compounds **5** and **6**.

The subcellular distribution of the methyl ester derivatives (e.g., compounds **3** and **4** in Fig. 4) changing from ER/mitochondria to granular structures has been noted previously for compound **2** in the murine RIF sarcoma cells[30]. The latter sub-cellular distribution had been attributed to a deposition of compound **2** into the golgi compartment[30]. The technique previously used to determine golgi association involved staining cells with the golgi-specific tracking dye BODIPY-C5-ceramide. However, this technique proved to introduce an artefactual interaction with pyropheophorbides with the dye. Incubation of either tumor epithelial cells or fibroblasts for 30 minutes with PODIPY-C5-ceramide led to the specific fluorescent labeling of the Golgi complexes as designed. Concurrent with PODIPY-C5-ceramide deposition in the Golgi membranes, an immediate redistribution of already internalized and mitochondrially localized pyropheophorbides to the Golgi structures was triggered resulting in a congruent co-localization of the fluorescence of the Golgi tracker and pyropheophorbide (Baumann *et. al*., unpublished results).

Hence, a re-evaluation of the subcellular localization has been carried out by using organelle-directed deposition of fluorescent proteins that do not interfere with tetrapyrolic

compounds, such as analyzed in this study. The deposition sites of the compounds **2** and **2a** are demonstrated in the example of matrix- adherent tumor fibroblasts (Fig. 5).

While compound **2a** shows substantial overlap with both ER and mitochondrial markers, compound **2** indicates only minimal co-localization with ER, mitochondrial and lysosomal markers and virtually none with golgi and peroxisomes. These findings are in part in agreement with the data established for Colon26 cells by ima ge-stream analysis (Fig. 3B & C). Close inspection of microscopic images of fibroblasts (Fig. 5) indicates that most of the structures binding compounds **2, 3**, and **4** represent optically dense vesicles. These vesicles appear neutral in charge because these are not stained by lysotracker and are distinct from ER, golgi and mitochondria. The precise identity of the target structures binding the methyl ester derivatives remains to be determined.

The same uptake studies as presented for fibroblasts in Figs 4 & 5, have been carried out with primary cultures of lung tumor epithelial cells (data not shown, see related information in Figs. 6–9 below). The results indicate that the isomeric compounds, similar to the mixture of the isomers in compounds **2** and **2a**, have the same uptake and subcellular distribution patterns as described for fibroblasts. However, a major difference exists in retention properties. The release kinetics for all compounds is slower than determined for fibroblasts, which, depending on the particular epithelial cell culture, results in a half-life of 24 to 48 hours for compounds **2, 3** and **4** and a half-life of 6 to 24 hours for compounds **2a, 5** and **6**. As noted for fibroblasts, the subcellular localization of the methyl ester derivatives (e.g., compound **2**) in the epithelial cells is distinct from lysosomes, golgi and peroxisomes.

2.3. *In vitro* tumor cell-specificity of photosensitizers: Methyl ester vs. carboxylic acid derivatives

The distinct release kinetics of the compounds by fibroblasts and epithelial cells implies that these compounds in the context of tumor tissue will yield a tumor cell-specific retention. To determine whether this indeed applies to the compounds under investigation and whether an isoform-specific property exists, we tested each compound in a reconstituted co-culture system composed of primary human lung tumor stromal and epithelial cells. To facilitate identification of the cell types over the course of the experiment, the stromal fibroblasts were marked with green vital stain carboxyfluorescein succinimidyl ester (CSFE) prior to the addition to pre-established cultures of matrix-adherent epithelial cells. The representative example for compounds **2** and **2a** in Fig. 6 documents the key features. Although the co-cultured cells take up the compounds similarly, during the subsequent culture period in the absence of the compounds, fibroblasts show an accelerated loss of the compounds distinguishable from the prolonged retention by the tumor cells. The comparison of compounds also confirms that while the carboxylic acid derivatives consistently are taken up at higher amounts than the methyl ester derivatives, the loss rate of the carboxylic acid derivatives from most epithelial cell preparations is also higher. These cell type-specific properties result in differential display of the compounds during the course of treatment with initial prominence of carboxylic acid derivatives in tumor cells (e.g., after 6 hours in Fig. 6) that changes to a more notable persistence of the methyl ester derivatives at later stage (e.g., 24 hours in Fig. 6).

The relative pattern of compounds' uptake as shown in Fig. 6 was not restricted to the squamous carcinoma-derived cells used in this particular experiment but was similarly reproduced in essentially all other epithelial cell cultures derived from lung adenocarcinomas and squamous carcinomas (tested over 200 cases). For all cultures, the uptake of compound **2a** exceeded that of compound **2** by a factor of 2–5. These cultures, however, showed variable loss rates of carboxylic acid derivatives compared to the methyl ester derivatives. Cultures differed in retention of compound **2a**, ranging from maintaining concentration still exceeding compound **2** after 48-hour chase period to having non-detectable level already after 24-hour chase. Detailed analyses of 56 consecutive lung cancer cases for uptake and retention of pyropheophorbides detected four adenocarcinoma cases that presented an exceptionally high relative loss rate for derivatives with 17^2 carboxylic acid group (half-life <12 hours) that equalled the rate determined for fibroblasts. The particular effective egress correlated with the induced expression of ABCG2 transport protein in these lung cancer cells[41,42]. Most of the primary cell cultures generated from lung tumor tissue, both fibroblastic and epithelial cells, did not show immune-detectable expression of ABCG2 protein.

To prove that the specific transport of ABCG2 also applied to the carboxylic acid derivatives, but not methyl ester derivatives of the compounds of this study, the retention of these was measured in tumor epithelial cells with the highest expression of ABCG2 (L352) as a function of treatment with imatinib mesylate, an inhibitor of ABCG2 activity (Fig. 7)[42]. While the tumor cells exported essentially all compound **2a** within 4-hour chase period in the absence of imatinib, the cellular content of compound **2a** was maintained high in the presence of the inhibitor. The ABCG2 substrate function did not appreciably apply to compound **2**. These results suggest that tumor-specific expression of ABCG2 contributes to the pyropheophorbide retention and, thus, to the potential effectiveness of PDT.

2.4. Chirality at position-3 in compounds 2 and 2a affects cellular uptake and retention

Previous structure activity relationship (SAR) and quantitative structure activity relationship (QSAR) studies of a series of pyropheophorbides from our laboratory have shown that overall lipophilicity of the molecule makes a significant difference in PDT efficacy[16,17, 44–47]. However, most of the highly effective compounds selected so far were isolated as racemic mixtures due to introduction of the chiral center at position-3 (IUPAC nomenclature). This is also the case for compounds **2** and **2a** as a consequence of ring D reduction in *trans*- (absolute *trans*-configuration). To evaluate the importance of the chiral center at this position for the biological effects we had determined, 3-(1'-*m*-iodobenzyloxymethyl)pyropheophorbide-a (compounds **9**) was synthesized by following the methodology depicted in Scheme 1. Both the methyl ester (compound **9**) and the carboxylic acid derivative (compound **9a**) were evaluated for *in vitro* and *in vivo* efficacy. *In vitro* uptake (influx, intracellular distribution and/or efflux) of compounds **9** and **9a**, was determined in primary lung tumor epithelial cells and compared to the corresponding chiral compounds **2** and **2a** (Fig. 8) The results indicate that uptake of compound **9** is comparable to that of compound **2** both in quantity and in the subcellular localization to granular structures (Fig. 8, **left panel**). However, retention of compound **9** is several-fold lower resulting in a preferential loss of it over the 24-hour culture period.

A similar functional assessment of the chiral center at position-3 in the carboxylic acid derivatives was made by comparing compound **9a** and compound **2a** in the same lung tumor cells (Fig. 8, right panel). While compound **2a** yielded the expected high level accumulation during the initial 4-hour uptake period that exceeded the level of compound **2** or **9** by 4-fold, compound **9a** was accumulated to a 10% level of compound **2a**. Despite this quantitative difference, both compounds **2a** and **9a** primarily co-localized to the ER/mitochondrial compartment. Compound **9a** was not only taken up at reduced level, but was also rapidly cleared from the cells with only traces detectable after 4-hour chase. Both compounds **2a** and **9a** contain a carboxylic acid group at position-17[2] a structure necessary for being a substrate for the ABCG2 transporter. Uptake and retention of compound **9a**, like that compound **2a**, is enhanced in cells expressing ABCG2 by treatment with the inhibitor Imatinib (Fig. 7).

These comparative analyses of the various derivatives highlighted the fact that not only the uptake but also cellular retention critically determines the actual cellular level of the photosensitizers. In the example of the lung epithelial cells, the time-dependent change in the compound's retention is a major determinant of cellular content of effective PS. While compound **2a** is dominant at early time points, the strong retention of compound **2** renders this photosensitizer to dominant at later time points. The level of photosensitizers, including all the compounds evaluated here, dictates the magnitude of photoreaction.

2.5. The cellular level of each compound correlates with the magnitude of photoreaction in vitro

The photosensitizing activity of the compounds was defined in cell cultures by following four PDT response assays: (i) the magnitude of photoreaction resulting in the dose-dependent oxidative dimerization of STAT3 (signal transduced and activator of transcription 3), (ii) immediate activation of the stress MAPK (p38) pathway, (iii) Loss of EGFR (epidermal growth factor) and (iv) reduced cell survival 24–hour post-PDT[48]. The quantitative assessment was made in independent preparations of lung tumor epithelial cells. Replicate sets of cultures were incubated for 4 hours with the various compounds, followed by a 4 hour chase period in compound-free medium to achieve an optimal subcellular accumulation specific for each compound (see example in Fig. 8). After recording the cell-associated compounds' fluorescence, the cells were exposed to therapeutic light at 665 nm and either immediately extracted for quantification of the homodimerized STAT3, phosphorylated (activated) p38, and EGFR by immunoblotting (Fig. 9B and C) or incubated for additional 24 hours to determine relative cell survival (Fig. 9D).

The cellular accumulation and subcellular localization of compounds **2** to **6** showed comparable patterns as noted for Colon26 cells (Fig. 3B) and fibroblasts (Fig. 4). There was no detectable difference between the two isoforms comprising the methyl ester and carboxylic acid derivatives. The cell-associated fluorescence of the accumulated compounds tightly correlates with the light-induced photoreaction leading to STAT3 crosslinking, p38 activation and EGFR loss (Fig. 9B & C). These immediate responses are proportionally reflected in mediating cell death. The analyses also indicate a distinct dose-dependent action for compounds **2** and **2a** (Fig. 9C & D) probably related to the distinct subcellular

localization and exchange kinetics for the two compounds. Despite these differences in uptake, the tight correlation of the amount of compounds present in the cells with the PDT response markers suggests that the distinct subcellular localization of the methyl ester and carboxylic acid derivatives and, thus, site of photoreaction, did not appreciably influence the cellular propagation of the oxidative reactions.

2.6. Comparative in vivo uptake and PDT efficacy of stereoisomers

Based on the information derived from the tissue culture analyses, uptake and clearance profiles of the isomers were investigated in BALB/c mice bearing Colon26 tumors. All compounds were intravenously injected at dose of 1 μmol/kg and its systemic distribution imaged at 24, 48 and 72 hours post-injection using the IVIS spectrum[48].

The results are summarized in Fig. 10 and indicate that maximal uptake of all the compounds is observed at 24 hour post-injection without significant difference between compound **2** (isomeric mixture) and the corresponding isomers **3** and **4** (*p* values: 24 h- 0.56; 48 h- 0.67; 72 h- 0.54). In line with the findings made in tissue culture systems, the corresponding carboxylic acid derivatives **5** and **6** showed similar uptake and pharmacokinetic profiles with maximal uptake at 24 h post-injection.

To further correlate the *in vivo* uptake of the compounds with *in vivo* PDT efficacy and tumor destruction, the initial experiment tested compound **2** at a constant dose, but using two different light fluence rates (135J/cm^2, 75 mW/cm^2 vs. 128J/cm^2, 14 mW/cm^2). From the results summarized in Fig. 11A, it can be seen that compound **2** is more effective when light is delivered at low fluence rate. Such an enhanced PDT efficacy by low fluence rates has also been reported by other investigators[49]. Therefore, the *in vivo* anti-tumor activity of the *R*- and *S*- isomers of methyl ester (**2**) and carboxylic acid (**2a**) analogs, were individually evaluated in BALB/c mice bearing Colon26 tumors by applying the more effective treatment regimen. The results indicated that the compound **2** and its isomers **3** and **4** are equally effective (Fig. 11B). Equivalent activity was also determined for compounds **5** and **6** (Fig. 11C). The similar PDT activity of methyl ester vs. carboxylic acid analogs suggests that the condition selected for the photosensitizer administration (i.e., drug concentration and 24-hour incubation period) has resulted in a comparable level of retention in tumor tissue and, thus, photoreaction

The same Colon26 tumor model also confirmed that compound **9** without chiral center is less effective than compound **2** with chiral center (Fig. 11D) in agreement with *in vitro* data (Fig. 9). In summary, this study clearly indicates that among aryl ether analogs, the presence of chirality at position-3 is of utmost importance, and is currently being explored in other tetrapyrrolic systems.

2.7. Comparative uptake of PS 2 vs. Photofrin in human tumor

The uptake studies involving primary cultures of lung tumor cells (e.g., Fig 6) suggested that certain lung cancer may be subjected to preferential killing by compound **2** due to its high retention by the tumor cells. Moreover, by simultaneous reduction of the photosensitizer level in stromal compartment, less collateral damage to these non-tumor cells may assist in

achieving an improved therapy. To test this possibility, we selected a non-small cell lung cancer that exhibited a preferential retention of compound **2** as was found in some primary tumor epithelial cultures (**e.g**, Figs. 6 & 8). The efficacy of compound **2** was compared to Photofrin™ (or Porfimer sodium), a photosensitizer that lack cell type specificity and also retained by stromal and epithelial cells (Fig. 12).

2.8. Application of ^{124}I- analogs of compound 12 and 13 for PET imaging

Based on the favorable *in vivo* PDT efficacy of compound **2**, it was decided to focus subsequent studies evaluating PET imaging ability on methyl ester derivatives. Therefore, the isomers **3** and **4** were converted into the corresponding ^{124}I- analogs **12** and **13** by following the methodology depicted in Scheme 1. Both isomers were obtained in 25–30% yield and >95% specificity. The imaging potential was determined in BALB/c mice bearing Colon26 tumors (3, 48 and 72 hours post-injection). The PET images showed similar systemic distribution and tumor uptake (Fig. 13). Optimal contrast was observed at 48 and 72 hours post injection when most of the ^{124}I-labeled compounds were cleared from most organs but were still retained at high level by the tumor. Since compounds **12** and **13** yielded identical imaging and therapeutic potential, we concluded that ^{124}I-compound **2** as an isomeric mixture could be used for cancer-imaging with an option of PDT when combining with the corresponding non-labeled analog to reach therapeutic concentration of the photosensitizing activity. To test the feasibility of achieving imaging *via* PET/fluorescence and effective PDT by a combination of compounds **12** (radioactive) and **2** (non-radioactive), BALB/c mice containing Colon26 tumors were injected first with 50 μCi of compound **12**. The mice were imaged at 24 hours and then non-labeled PS **2** at a dose of 1.0 μmol/kg (therapeutic dose) was injected. PET images were obtained at 24 hours later. No appreciable diminishment of tumor detection and loss of contrast were observed. At this stage, it would also be feasible to visualize the tumor by fluorescence to follow by application of therapeutic light dose. The successful application of this “See and Treat Approach” is currently in progress.

3. Experimental Section

3.1. Chemistry

All reactions were carried out in heat gun dried glassware under an atmosphere of nitrogen and magnetic stirring. Thin-layer chromatography (TLC) was used on precoated silica gel sheets (layer thickness: 0.25 mm) or aluminum oxide sheets. Column chromatography was performed either over silica gel 60 (70–230 mesh) or neutral alumina grade III. In some cases preparative TLC was ued for the purification of compounds. Solvents were dried following the standard methodology. ^{1}H and ^{13}C NMR spectra were recorded at room temperature in $CDCl_3$ solution using a Varian VNMRS-400 spectrometer. Compounds **1, 2, 2a**, were synthesized by following the literature procedure.[30] We followed Tamiaki’s approach[50] for the synthesis of compounds **7** and **8**,. and used for the preparation of compounds **9** and **9a** were characterized by NMR and elemental analysis. The purity of compounds **2, 3, 4** and **9** was also confirmed by HPLC analysis. All chemicals shifts are reported in parts per million (δ). ^{1}H NMR (400 MHz) spectra were referenced to residual $CHCl_3$ (7.26 ppm) or TMS (0.00 ppm). ^{13}C NMR (100 MHz) spectra was referenced to

$CDCl_3$ (77.0 ppm) or TMS (0.00 ppm). Mass spectrometry analysis were performed at the Mass Spectrometry Facility, Michigan State University, East Lansing. UV-visible spectra were recorded on FT UV-visible spectrophotometer using dichloromethane/THF as solvent.

3.2. Synthesis of methyl 3-devinyl-3-formyl pyropheophoride-a (7)

Methyl pyropheophoride-a **1** (100 mg) obtained following the literature procedure[37,38] was dissolved in THF. It was reacted with 20 mg OsO_4 (in CCl_4) and 200mg $NaIO_4$ (in H_2O and dioxane) and the reaction was stirred at room temperature for 2h.The reaction was monitored by UV (a shift from λ_{max}= 668nm to 695nm in CH_2Cl_2 was observed). 10% acetic acid (20 ml) was added to quench the reaction. It was then diluted with dichloromethane (200 mL) and washed with aqueous sodium bicarbonate and finally with water. The organic layer was then dried over anhydrous sodium sulfate. Evaporation of the solvent gave a residue which was purified by preparative plates, using 3% methanol/ dichloromethane as the eluting solvent, the major band was identified as desired product (75 mg, yield 74%). ^{1}H NMR (400 MHz, CDCl3, δ ppm): 11.55 (s, 1H, 3CHO), 10.30, 9.60, 8.84 (each s,1H, *meso*-H), 5.38 (d, *J*=20 Hz, 1H, 13^2CH_2), 5.23 (d, *J*=20 Hz, 1H, 13^2CH_2), 4.53–4.62 (m, 1H, 18H), 4.35–4.42 (m, 1H, 17H), 3.77 (s, 3H, for 17^2COOCH_3), 3.71 (m, 5H, $8CH_2CH_3$ and 1×ring CH_3), 3.62 and 3.31 (each s, 3H, for 2×ring CH_3), 2.69–2.79, 2.56–2.66, and 2.26–2.38 (m, 4H, $17^1$and 17^2H), 1.86 (d, *J*=6.8 Hz, 3H, $18CH_3$), 1.72 (t, J=7.2, 3H, $8CH_2CH_3$). MS calcd for $C_{33}H_{34}N_4O_4$:550.2. Found: *m/e* 551.2 (M+1).Anal. Calcd for $C_{33}H_{34}N_4O_4$: C, 71.98; H, 6.22; N, 10.17. Found: C, 71.75; H, 6.39; N, 10.09.

Synthesis of methyl 3-devinyl-3-hydroxymethyl pyropheophoride-a (8)—Methyl 3-devinyl-3-formyl-pyropheophoride-a (80 mg) in dry THF was reacted with $NaBH_4$ (100 mg), and the reaction was monitored by TLC. After the completion of reaction, the reaction mixture was poured in water (200 mL), extracted with dichloromethane (2 × 200 mL). The organic layer was separated, dried over anhydrous sodium sulfate, and the solvent was evaporated. The residue was purified by preparative plates, using 5% methanol/ dichloromethane as the eluting solvent. The major band was isolated and the title compound was obtained in 55% (55 mg) yield. ^{1}H NMR (400 MHz, CDCl3, δ ppm): 9.49, 9.43, 8.56 (each s, 1H, *meso*-H), 5.90 (s, 2H, $3CH_2OH$), 5.25 (d, *J*=20.8 Hz, 1H, 13^2CH_2), 5.10 (d, *J*=20.8 Hz, 1H, 13^2CH_2), 4.41–4.53 (m, 1H, 18H), 4.24–4.29 (m, 1H, 17H), 3.70 (q, *J*=8.0 Hz, 2H, $8CH_2CH_3$), 3.64, 3.61, 3.42 and 3.26 (each s, 3H, for 17^2COOCH_3 and 3×ring CH_3), 2.63–2.74, 2.51–2.58, 2.23–2.34 (m, 4H,17^1 and 17^2H), 2.14 (br s, 1H, $3CH_2OH$), 1.81 (d, J=7.6 Hz, 3H, $18CH_3$), 1.71(t, J=7.6 Hz, 3H, $8CH_2CH_3$), 0.26 (br s,1H, NH), −1.60 (br s, 1H, NH). MS Calcd. for $C_{33}H_{36}N_4O_4$: 552.2. Found: *m/e* 553.3 (M+1). Anal. calcd for $C_{33}H_{36}N_4O_4$: C, 71.72; H, 6.57; N, 10.14. Found: C, 71.03; H, 6.57; N, 9.76.

Synthesis of methyl 3-devinyl-3-{1'-(m-iodobenzyloxy)-methyl}pyropheophoride-a (9)—Compound **8** (50 mg) was reacted with 30% HBr/ acetic acid (1.5 mL), and stirred at room temperature for 1.5h. The HBr and acetic acid were removed under a high vacuum. The residue so obtained was immediately dissolved in dry CH_2Cl_2 (2 mL) and reacted with 3- iodobenzyl alcohol (200 μL) in the presence of anhydrous potassium carbonate (50 mg). The reaction mixture was stirred for 2 h at room temperature. After the standard work-up, the residue was purified by preparative plates,

using 4% methanol/dichloromethane, and the title compound was obtained in 30% yield (21 mg). ^{1}H NMR (400 MHz, CDCl3, δ ppm): 9.49, 9.39, 8.56 (each s,1H, *meso*-H), 7.83 (s, 1H, ArH), 7.66 (d, *J*=7.7 Hz, 1H, ArH), 7.40 (d, *J*=7.6 Hz, 1H, ArH), 7.10 (t, *J*=7.7 Hz, 1H, ArH), 5.72 (s, 2H, $3^{1}CH_2$), 5.26 (d, *J*=19.8 Hz, 1H, $13^{2}CH_2$), 5.11 (d, *J*=19.8 Hz, 1H, $13^{2}CH_2$), 4.74 (s, 2H, OCH_2Ar), 4.49 (q, *J*=7.0 Hz, 1H, 18H), 4.30 (m, 1H, 17H), 3.68 (q, *J*=7.8 Hz, 2H, $8CH_2CH_3$), 3.65, 3.61, 3.36 and 3.19 (each s, 3H, for $17^{2}COOCH_3$ and 3×ring CH_3), 2.63–2.75, 2.50–2.62, and 2.22–2.35 (4 × m, 4H, 2 × 17^{1}H and 2 × 17^{2}H), 1.81 (d, J=7.1 Hz, 3H, $18CH_3$), 1.69 (t, 3H, J=7.6 Hz, $8CH_2CH3$), 0.33 (br s,1H, NH), −1.78 (br s, 1H, NH). ^{13}C NMR (100 MHz, $CDCl_3$, **5** ppm): 196.2, 173.5, 171.3, 160.3, 155.1, 150.9, 148.9, 145.0, 141.1, 140.6, 137.9, 136.9, 136.9, 136.5, 136.2, 134.7, 133.7, 130.6, 130.3, 128.5, 127.1, 106.2, 104.0, 97.1, 94.5, 93.2, 71.2, 63.3, 51.7, 51.7, 50.0, 48.1, 30.9, 29.9, 23.2, 19.5, 17.5, 12.1, 11.4, 11.3. MS calcd for C40H41O4N4I: 768.2. Found: *m/e* 791.5 (M+23).

Isomer (3)—UV-visible, $\lambda_{max}(CH_2Cl_2)$, nm (£):661, 613 605, 536, 407. ^{1}H NMR (400 MHz, CDCl3, **5** ppm): 9.75, 9.55, 8.55 (each s,1H, *meso*-H), 7.75 (br s, 1H ArH), 7.63 (d, *J*=7.6 Hz, 1 H, ArH), 7.28 (d, *J*=7.6 Hz, 1 H, ArH), 7.05 (t, *J*=7.7 Hz 1 H, ArH), 5.98 (q, J=6.7 Hz, 1H, 3^{1}H), 5.27 (d, *J*=19.9 Hz, 1H, $13^{2}CH_2$), 5.12 (d, J=19.9 Hz, 1H, $13^{2}CH_2$), 4.54 & 4.68 (each d, *J*=11.9 Hz, 1H, OCH_2Ar), 4.50 (dq, *J*=7.4, ~1.7 Hz, 1 H, 18H), 4.31 (m, 1H, 17H), 3.72 (q, *J*=7.6 Hz, 2H, $8CH_2CH_3$), 3.69 (s, 3H, $17^{2}CO_2CH_3$), 3.60, 3.37, 3.21 (each s, 3H, ring CH_3), 2.65–2.76, 2.51–2.61, 2.21–2.38 (4 × m, 4H, 17^{1} & 17^{2}H), 2.17 (d, *J*=6.7 Hz, 3H, $3^{1}CH_3$), 1.82 (d, *J*=7.2 Hz, 3H, $18CH_3$), 1.71 (t, *J*=7.6 Hz, 3H, $8CH_2CH_3$), 0.40 (br s, 1H, NH), −1.73 (br s, 1H, NH). ^{13}C NMR (100 MHz, $CDCl_3$, **5** ppm): 196.1, 173.4, 171.3, 160.2, 155.1, 150.9, 148.9, 145.0, 141.1, 140.6, 138.3, 137.8, 136.9, 136.7, 136.3, 135.2, 132.6, 130.5, 130.1, 128.4, 127.1,106.0, 104.1, 97.8, 94.4, 92.7, 72.0, 70.2, 51.6, 51.6, 49.9, 48.0, 30.8, 29.8, 24.5, 23.1, 19.4, 17.4, 12.0, 11.3, 11.0. HRMS calcd. for $C41H_{43}IN_4O4$ 783.2407 (M + H); Found, 783.2411.

Isomer (4)—UV-visible, $\lambda_{max}(CH_2Cl_2)$, nm (£):661, 613 605, 536, 407: ^{1}H NMR (400 MHz, CDCl3, **5** ppm): 9.74, 9.55, 8.55 (each s,1H, *meso-H)*, 7.75 (br s, 1H ArH), 7.63 (d, *J*=7.9 Hz, 1H, ArH), 7.29 (d, *J*=7.7 Hz, 1H, ArH), 7.05 (t, *J*=7.7 Hz, 1H, ArH), 5.98 (q, J=6.7 Hz, 1H, 3^{1}H), 5.27 (d, *J*=19.8 Hz, 1H, $13^{2}CH_2$), 5.12 (d, *J*=19.8 Hz, 1H, $13^{2}CH_2$), 4.68 & 4.55 (each d, *J*=11.9 Hz, 1 H, OCH_2Ar), 4.49 (dq, *J*=7.4, ~1.9 Hz, 1H, 18H), 4.31 (m, 1H, 17H), 3.71 (q, *J*=7.6 Hz, 2H, $8CH_2CH_3$), 3.69 (s, 3H, 17^{2} CO_2CH_3), 3.60, 3.37, 3.20 (each s, 3H, for 3 × ring CH_3), 2.64–2.75, 2.50–2.60, 2.20–2.37 (4 × m, 4H, 17^{1} & 17^{2}H), 2.16 (d, J=6.7 Hz, 3H, $3^{1}CH_3$), 1.82 (d, *J*=7.3 Hz, 3H, $18CH_3$), 1.71 (t, *J*=7.6 Hz, 3H, $8CH_2CH_3$), 0.39 (br s, 1H, NH), −1.74 (br s, 1H, NH). ^{13}C NMR (100 MHz, $CDCl_3$, δ ppm): 196.1, 173.4, 171.3, 160.3, 155.1, 150.9, 148.9, 145.0, 141.0, 140.7, 138.3, 137.8, 136.9, 136.7, 136.3, 135.2, 132.7, 130.5, 130.1, 128.4, 127.1, 106.0, 104.1, 97.8, 94.4, 92.7, 72.0, 70.2, 51.6, 51.6, 49.9, 48.0, 30.8, 29.8, 24.5, 23.1, 19.4, 17.4, 12.0, 11.3, 11.0. HRMS calcd for $C_{41}H_{43}IN_4O_4$ 783.2411 (M + H); Found, 783.2407.

4.1.5. Isomer (5): ^{1}H NMR (400 MHz, $CDCl_3$, δ ppm): 9.73, 9.51, 8.55 (each s,1H, *meso*-H), 7.74 (br s, 1H ArH), 7.62 (d, *J*=7.9 Hz, 1H, ArH), 7.27 (d, *J*~8 Hz, 1H, ArH), 7.03 (t, *J*=7.8 Hz, 1H, ArH), 5.96 (q, *J*=6.7 Hz, 1H, 3^{1}H), 5.27 (d, *J*=19.9 Hz, 1H, $13^{2}CH_2$), 5.13 (d,

J=19.9 Hz, 1H, 13^2CH_2), 4.66 & 4.52 (each d, *J*=11.9 Hz, 1H, OCH_2Ar), 4.50 (dq, *J*~7.5, 1.6 Hz, 1H, 18H), 4.33 (m, 1H, 17H), 3.70 (q, *J*=7.6 Hz, 2H, $8CH_2CH_3$), 3.65, 3.35, 3.20 (each s, 3H, for 3 × ring CH_3), 2.56–2.76, 2.22–2.35 (4 × m, 4H, 17^1 & 17^2H), 2.16 (d, *J*=6.7 Hz, 3H, 3^1CH_3), 1.82 (d, *J*=7.3 Hz, 3H, $18CH_3$), 1.70 (t, *J*=7.7 Hz, 3H, $8CH_2CH_3$), 0.88 (brs, 1H, NH) −1.70 (brs, 1H, NH).

4.1.6.Isomer (6): ^{1}H NMR (400 MHz, CDCl3, δ ppm): 9.73, 9.53, 8.55 (each s,1H, *meso*-H), 7.75 (br s, 1H ArH), 7.63 (d, *J*=8.0 Hz, 1H, ArH), 7.29 (d, *J*=7.8 Hz, 1H, ArH), 7.05 (t, *J*=7.7 Hz, 1H, ArH), 5.97 (q, *J*=6.7 Hz, 1H, 3^1H), 5.28 (d, *J*=19.9 Hz, 1H, 13^2CH_2), 5.13 (d, *J*=19.9 Hz, 1H, 13^2CH_2), 4.68 & 4.54 (each d, *J*=11.9 Hz, 1H, OCH_2Ar), 4.50 (q, *J*=7.3, ~1.5 Hz, 1H, 18H), 4.34 (m, 1H, 17H), 3.70 (q, 7.6 Hz, 2H, $8CH_2CH_3$), 3.67, 3.36, 3.19 (each s, 3H, for 3 × ring CH_3), 2.56–2.78, 2.24–2.37 (4 × m, 4H, 17^1 & 17^2 H), 2.15 (d, *J*=6.7 Hz, 3H, 3^1CH_3), 1.82 (d, *J*=7.2 Hz, 3H, $18CH_3$), 1.70 (t, *J*=7.6 Hz, 3H, $8CH_2CH_3$), −1.71 (br s, 1H, NH). ^{13}C NMR (100 MHz, $CDCl_3$, δ ppm): 196.4, 177.1, 171.3, 160.2, 155.2, 150.9, 149.0, 145.0, 141.1, 140.6, 138.3, 137.8, 136.9, 136.7, 136.4, 135.3, 132.7, 130.4, 130.1, 128.4, 12.1, 106.0, 104.1, 97.8, 94.43, 92.7, 71.9, 70.2, 51.5, 49.9, 47.9, 30.5, 29.6, 24.5, 23.1, 19.4, 17.4, 12.0, 11.3, 11.1.

Trimethyl tin analogs

Isomer (10): The solution of **3** (9.0 mg, 0.01 mmol, 1.0 equiv.) in dry THF were added hexamethydistannane (35.0 μL) and bis(triphenylphosphine) palladium(II)dichloride (2.86 mg, 0.004 mmol, 0.4 equiv.), and the reaction mixture was stirred at room temperature under argon for overnight. The solvent was evaporated. The crude product was purified by preparative plates using 50% ethyl acetate/hexanes to give isomer **10**. Yield: 5.6 mg (59%), UV-visible, $\lambda_{max}(CH_2Cl_2)$, nm (ε):661, 613 605, 536, 407: ^{1}H NMR (400 MHz, CDCl3, **5** ppm): 9.76, 9.54, 8.54 (each s, 1H, *meso-H)*, 7.30–7.46 (m, 4H, ArH), 6.01 (q, *J*=6.7 Hz, 1H, 3^1H), 5.27 (d, *J*=19.8 Hz, 1H, 13 $^2CH_2$), 5.12 (d, *J*=19.8 Hz, 1H, 13 $^2CH_2$), 4.76 & 4.59 (each d, *J*=11.6 Hz, 1H, OCH_2Ar), 4.49 (q, *J*=7.3 Hz, 1H, 18H), 4.31 (d, *J*=8.1 Hz, 1H, 17H), 3.67–3.74 (5H, 3H of 17^2 CO_2CH_3 and 2H of $8CH_2CH_3$), 3.61, 3.37, 3.17 (each s, 3H, for 3 × ring CH_3), 2.66–2.74, 2.52–2.60, 2.19–2.37 (4 × m, 4H, 17^1 & 17^2H), 2.15 (d, *J*=6.7 Hz, 3H, 3^1CH_3), 1.82 (d, *J*=7.2 Hz, 3H, $18CH_3$), 1.71 (t, 3H, *J*=7.6 Hz, $8CH_2CH3$), 0.46 (br s, 1H, NH), 0.19 (s, 9H, $Sn(CH_3)_3$, −1.70 (br s, 1H, NH). ^{13}C NMR (100 MHz, $CDCl_3$, **5** ppm): 196.1, 173.4, 171.3, 160.1, 155.2, 150.9, 148.9, 144.9, 142.4, 141.2, 138.9, 137.8, 137.6, 136.3, 135.5, 135.4, 135.2, 132.5, 130.4, 128.3, 128.2, 128.0, 105.9, 104.1, 97.9, 92.6, 71.6, 71.4, 51.6, 51.6, 49.9, 48.0, 30.8, 29.8, 24.5, 23.1, 19.4, 17.4, 12.0, 11.2, 11.0, −9.6. HRMS calcd for $C_44H5_2N_4O4Sn$, 821.3089 (M + H); Found, 821.3110.

Isomer (11): Compound **4** (8.0 mg, 0.01mmol (1.0 equiv), in dry THF was added to hexamethydistannane (35.0 μL) and bis(triphenylphosphine) palladium(II)dichloride (3.2 mg, 0.004 mmol, 0.4 equiv.). The reaction mixture was stirred at room temperature under argon for overnight. The solvent was evaporated. The crude product was purified by preparative plates using 50% ethyl acetate/heaxane, and the desired compound was isolated in 48% (4.0 mg) yield. UV-visible, $\lambda_{max}(CH_2Cl_2)$, nm (ε):661, 613 605, 536, 407: ^{1}H NMR (400 MHz, CDCl3, **5** ppm): 9.75, 9.54, 8.54 (each s, 1H, *meso*-H), 7.33–7.43 (m, 4H, ArH), 6.00 (q, *J*=6.8 Hz, 1 H, 3^1 H), ~5.27 (d, 1H, 13^2CH_2), 5.11 (d, *J*=19.7 Hz, 1H, 13^2CH_2),

4.76 & 4.59 (each d, *J*=11.7 Hz, 1H, OCH_2Ar), 4.49 (dq, *J*=7.4 Hz, ~1.9 Hz, 1H, 18H), 4.30 (m, 1H, 17H), 3.65–3.74 (5H, 3H of $17^2CO_2CH_3$ and 2H of $8CH_2CH_3$), 3.60, 3.35, 3.16 (each s, 3H, for 3 × ring CH_3), 2.64–2.75, 2.50–2.60, 2.20–2.37 (4 × m, 4H, 17^1 & 17^2H), 2.14 (d, *J*=6.7 Hz, 3H, 3^1CH_3), 1.81 (d, *J*=7.4 Hz, 3H, $18CH_3$), 1.70 (t, *J*=7.7 Hz, 3H, $8CH_2CH_3$), 0.44 (br s, 1H, NH), 0.18 (s, 9H, $Sn(CH_3)_3$), −1.71 (br s, 1H, NH). ^{13}C NMR (100 MHz, $CDCl_3$, δ ppm): 196.2, 173.4, 171.37, 160.2, 155.2 150.9, 149.0, 144.9, 142.5, 141.2, 138.8, 137.8, 137.6, 136.3, 135.6, 135.5, 135.2, 132.6, 130.5, 128.3, 128.3, 128.0, 106.0, 104.1, 97.9, 92.6, 71.6, 71.4, 51.6, 51.6, 50.0, 48.0, 30.8, 29.8, 24.5, 23.1, 19.5, 17.4, 12.1, 11.3, 11.1, −9.62. HRMS calcd. for $C_{44}H_{52}N_4O_4Sn$: 821.3089 (M + H); Found, 821.3098 (M + H).

Synthesis of 3-devinyl-3-{1'-(m-iodobenzyoxy)-methyl} pyropheophoride-a carboxylic acid (9a): Methyl 3-devinyl-3-{1'-(*m*-iodobenzyoxy)-methyl} pyropheophoride-a **9** (50 mg) was reacted with 70 mg aqueous LiOH in THF (10 mL), and the reaction was stirred at room temperature for 3 h. After the standard work-up, the residue was purified by preparative plates, using 4% methanol/dichloromethane as the eluting solvent, and the desired compound was obtained in 70% yield (34 mg) ^{1}H NMR (400 MHz, CDCl3, δ ppm): 9.36, 9.23, 8.46 (each s, 1H, *meso*-H), 7.75 (s, 1H, ArH), 7.6 (d, *J*=8.0, 1H, ArH), 7.35 (d, *J*=7.20, 1H, ArH), 7.04 (t, *J*=8.0, 1H, ArH), 5.62 (s, 2H, $3CH_2$), 5.17 (d, *J*=20, 1H, 13^2CH_2), 5.05 (d, *J*=20, 1H, 13^2CH_2), 4.68 (s, 2H, OCH_2Ar), 4.40 (m, 1H, 18H), 4.20 (m, 1H, 17H), 3.57 (q, *J*=8.0, 2H, $8CH_2CH_3$), 3.54, 3.26, 3.09 (each s, 3H, for 3×ring CH_3), 2.51–2.67, 2.22–2.39, and 2.06–2.19 (4 × m, 4H, 17^1 and 17^2H), 1.73 (d, *J*=6.0, 3H, $18CH_3$), 1.60 (t, *J*=7.6, 3H, $8CH_2CH_3$). MS calcd for $C_{39}H_{39}O_4N_4I$: 754.2. Found: 754.4. HRMS, Calcd for $C_{39}H_{40}N_4O_4I$ (MH): 755.2096, Found 755.2075.

General method for the synthesis of ^{124}I- compounds (12 and 13): The trimethyl tin isomers **10** and **11** (60 μg) were individually dissolved in 5% acetic acid in methanol (50 μL) and added to a tube containing dried $Na1^{24}I$ (60 ng). To this solution was added 10 μL of *N*-chlorosuccinimide (1 mg/mL in methanol). The reaction mixture was left at room temperature for 8 min. It was then loaded in HPLC column (symmetry C18 5μm, 4.6 mm × 150 mm), and eluted with methanol/water (88:12). The flow rate was adjusted to 1 mL/min, and the UV detector was set at 254 nm. The labeled product was collected and the solvents were evaporated under nitrogen gas flow. The product was re-dissolved in 10% ethanol/ saline solution for in vivo experiments. The radiochemical yield was 30%, with specific activity > 1 Ci/μmol. The purity of each isomer was confirmed again by HPLC.

3.3. Cell cultures

Analyses of the compounds were carried out with two types of cells: Colon26 murine colon tumor cells as described previously and primary cultures of fibroblasts and epithelial cells from human lung tumor tissue[36]. Surgical lung specimens were provided by RPCI tissue procurement service and were processed to recover monotypic cultures of epithelial and stromal fibroblast following published procedures[36]. Proliferating epithelial cells (all labeled by the number of lung tumor sample registered in the laboratory records, e.g., "L370-T-EC") were maintained on collagen-1-matix in keratinocyte serum-free medium (KSFM) supplemented with growth factor and cholera toxin (Live Technologies). Fibroblast cultures

from the same tumor tissue (e.g., L370-T-Fb) were established in DMEM containing 10% fetal bovine serum (FBS). Subcultures (passage 2–4) of either cell type were used for testing uptake of the compounds and PDT action. To achieve comparable conditions among these cultures, the cellular fate of the compounds were determined in cultures incubated with DMEM with 10% FBS. Tumor-relevant co-cultures of stromal and epithelial cells were generated as follows. Tumor epithelial cells were plated at 1/20 dilution onto collagen-1-coated 6-well cluster plates in KSFM. After 2 days, fibroblasts were added to the epithelial cells with simultaneously switch to DMEM containing 10% FBS. In selected experiments, the fibroblasts were marked prior addition to the epithelial cells by tagging with CSFE. Since most primary epithelial cell cultures derived from tumor tissue could not be maintain beyond few passages, several long-term primary cultures were generated from squamous carcinomas and adenocarcinoma xenografts passaged at least 3 times in SCID mice. Initial cell cultures derived from xenografts (passage 0) were used to identify the profile of photosensitizer retention. Subsequent passages of these cultures, without subjecting to any immortalization procedures, were adapted to growth in DMEM containing 10% FBS (labeled as “TEC”). Aliquots of these TEC cultures were also used to inoculate SCID mice for generating *in vivo* tumors for defining photosensitizer uptake and PDT.

3.4. Organelle tracking

To identify subcellular localization of the compounds, cells were either stained for mitochondria and lysosomes with MitoTacker-Green and LysoTracker-Green (Life Technologies) or transduced with baculovirus-based expression CellLight® vectors for organelle-targeted fluorescent protein Golgi-GFP, ER-GFP or peroxisome-RFP (Life Technologies). Transduced cultures were subdivided after 24 hours into 6-well cluster plates and used 24 hours later for uptake of compounds.

3.4. In vitro uptake and detection of compounds

Cell cultures were incubated with medium containing different concentrations of compounds for periods ranging from 30 min to 24 hours. The cells were washed with cold, serum-free medium. Depending on the experimental setting, cultures were immediately monitored for the amount of uptake or were subjected to continued culture in compound-free medium containing 10% FBS (termed “chase”). Cell-associated compounds were visualized by fluorescent microscopy of the live cultures using either a Zeiss Axiovert or Nikon Eclipse Ti instrument. The fluorescence was digitally recorded as monochrome images and quantitated by integration using ImageQuant program (GE-Healthcare Life Sciences). The fluorescence was expressed in arbitrary fluorescent units[36] and normalized to cell protein measured for the cultures. For pictorial presentation, the fluorescent signals for organelle trackers were colorized in green and the signals for photosensitizers in red.

3.5. Cytometry

Samples of Colon26 cells were analyzed by flow cytometry using an ImageStream^{x} instrument (Amnis). The instrument utilizes 5 excitation lasers and is able to detect the fluorescence at 12 emission wavelengths, along with recording bright field images of individual cells. Both the intensity and location of fluorescent probes can be quantified. By

using compartment-specific stains (CMX-ROS - mitochondria; Fluorospheres - lysosomes), the overlap of the pyropheophorbide fluorescence with that of the stained subcellular organs were established. These regions were then identified (using masks) and IDEAS software was used to quantitate the amount of drug in each of these compartments. The IDEAS software algorithms evaluates the co-localization of the drug and the specific stain within each compartment. The more positive similarity score suggests that the particular site is more associated with the PS in that specific site. Data are expressed as mean ± SD arbitrary fluorescence units of replicate samples or mean ±SD similarity score ranking.

3.6. Cell analyses

Cell cultures incubated with compounds were treated at 37 °C with 665 nm light from an argon pumped dye laser at a fluence rate of 5 mW/cm^2 to a fluence of 3 J/cm^2. The cells were either immediately extracted in RIPA lysis buffer[36] or incubated for additional 24 hours in growth medium. Surviving cells were determined by releasing the cells from the culture substratum by trypsin digestion and counting viable cells based on trypan blue exclusion. The survival was expressed in percent of viable cells relative to the control cultures (exposed to the light only). An alternative assay of cell survival of Colon26 cells involved a treatment of cells in 96-well cluster plates with the laser light followed by 48-hour incubation in complete medium. The cultures were incubated with 10 μL/well of 4 mg/mL MTT for the final 4h. The MTT-containing medium was removed and 100 μL DMSO was added to solubilize the formazan crystals. The absorbance of the wells was read on a microliter plate reader at a wavelength on 500 nm. The results were expressed as present relative to the controls.

Cell lysates were subjected to western blot analysis for marker proteins as described[36]. The samples containing equal amounts of proteins were separated on SDS polyacrylamide gels. The proteins were transferred onto nitrocellulose membranes and reacted with antibodies against STAT3 (Santa Cruz Biotechnologies, Santa Cruz, CA), EGFR, phospho-p38 or total p38 (Cell Signalling Technologies, Inc. Danvers, MA). The immune complexes were visualized by reaction with peroxidase-conjugated secondary antibodies followed by enhanced chemiluminescence (ELC) (Pierce Chemical, Rockford, IL). The ELC signals were recorded on X-ray films and quantified as described[36]. The crosslinking of STAT3 was expressed as the fraction of the integrated ELC signal for the homodimerized STAT3 (equal the cross linked STAT3 complex I) relative to the sum of the signals recorded for the homodimeric and monomeric STAT3.

3.7. Tumor-bearing mice and in vivo PDT

BALB/c mice (10 mice/group) were injected subcutaneously on the shoulder with 1 × 10^5 Colon26 cells in 50 μL of α-MEM. For lung tumor model, patient-derived non-small cell lung cancer (NSCLC) xenografts were established subcutaneously in SCID mice. Tissue fragments (1 mm^3) were implanted by trocar in the right shoulder. When tumors were approximately 5 mm × 5 mm (8–10 days post implantation), mice were randomized into control and treatment groups and injected intravenously with photosensitizers in 1% Tween80/D5W at the selected dose (generally 1 μmol/kg) in approximately 0.2 mL. After 24 hours, mice were restrained without anesthesia in Plexiglas holders designed to expose the

tumor area to light. Depending upon the photosensitizer used, the tumors were treated with laser light[50] at 665 nm for total fluence of 128 J/cm^2 at a fluence rate of 14 mW/cm^2 or 135 J/cm^2 at 75mW/cm^2, or with 630 nm light for a total fluence of 135 J/cm^2 at a fluence rate of 75 mW/cm^2. Following treatment, the tumor dimensions (orthogonal diameters) were measured by caliper every other day for tumor growth/regrowth assays. The tumor volume *V*, was calculated with the formula $V = (Iw^2/2)$, where I is the longest axis of the tumor and *w* is the axis perpendicular to *I*. Mice were euthanized when tumors reached the endpoint volume of 400 mm^3. Mice were considered cured if there was no palpable tumor by day 60. Results were plotted using Graph Pad Prism 5 and expressed as % tumor cures-the percent of mice with tumors less than 400 mm^3 at day 60.

3.8. In vivo tumor-imaging

All compounds were intravenously injected at dose of 1 μmol/kg (therapeutic dose) and its systemic distribution imaged at 24, 48 and 72 hours post-injection using the IVIS spectrum (Perkin-Elmer) along with Living Image (image acquisition and analysis software) IVIS Spectrum has the capability to use either trans-illumination (from the bottom) or epi-illumination (from the top) to illuminate *in vivo* fluorescent sources. The instrument is equipped with 10 narrow band excitation filters (30 nm bandwidth) and 18 narrow band emission filters (20 nm bandwidth) that assist in significantly reducing autofluorescence by the spectral scanning of filters and the use of spectral unmixing algorithms. Regions of interest (ROI) are defined for areas of compound accumulation (tumor, skin, organs) and total and average signals within the regions are recorded. Fluorescent intensity is expressed as the total radiant efficiency ([p/s] / [μW/cm2]. Results are expressed as mean total radiant efficiency of three mice ±SD.

3.9. PET Imaging

Mice (BALB/c mice bearing Colon26 tumors) were imaged in the microPET Focus120, a dedicated 3-dimensional small animal PET scanner (Concorde Microsystems Inc.) at SUNY, Buffalo using the approved ICAUC animal protocol. All mice (9 mice/group) were injected *via* a tail vein with 50 μCi of ^{124}I-PS **2** and the respective isomers **12** and **13**. Mice were imaged at 24, 48 and 72 hours post injection the acquisition time set for 30 min. No efforts were made to block the radioiodine uptake by thyroid or stomach, and surprisingly, in only a few cases was minor radioiodine uptake observed in the thyroid that cleared by 72 hours. After imaging the mice at each time-point, 3 mice were sacrificed and the tumors were removed and the total-uptake of the compounds by measuring the radioactivity. Radioactivity uptake was expressed as the percentage of the injected dose per gram of the tumor (%ID/g). Statistical analysis data (5ID/g vs time point) were plotted using GraphPad Prism 5.

4. Conclusion

Chirality is a prominent feature of most biological processes, and the isomers of a bioactive molecule often possess different biological effects. Drugs that are derived from natural products are usually obtained in the optically active pure form of a single isomer. However, drugs produced by chemical synthesis are usually a mixture of two or more isomers. The

results summarized in this manuscript for methyl 3-(1'-*m*-iodobenzyloxy)ethyl-3-devinylpyropheophorbide-a clearly indicate that compared to the isomeric mixture, the corresponding *pure* isomers (racemates) showed similar uptake, and in vivo PET and fluorescence imaging efficacy was optimal at 24 hour post-injection. Compared to methyl esters (position-17^2) the corresponding carboxylic acid analogs showed higher uptake and more specificity to mitochondria, but was also cleared with higher rate, hence mediated a comparable PDT reaction and the long-term cancer cures. However, eliminating the chirality at position-3^1 of PS **2** by introducing a non-chiral group in PS **9** (without any significant difference in overall lipophilicity, log p) considerably diminish cellular retention and *in vivo* PDT efficacy, which is surprising and warrants further investigation, *e.g*. comparative interaction with various sites of human serum albumin (HSA)[51,52] which has previously shown a direct correlation between the Site-II (HSA) binding of certain PS and PDT efficacy.

Due to similar PDT efficacy between the pure isomers **3, 4** and **5, 6** purified from the isomeric mixtures **2** and **2a** respectively, a correlation between the biological efficacy of individual isomers could not be confirmed. For establishing such a correlation, a detailed biological investigation on a series of isomerically pure alkyl/aryl ether analogs is in progress.

Supplementary Material

Refer to Web version on PubMed Central for supplementary material.

Acknowledgements

The help rendered by Dr. Yihui Chen in highly appreciated. We are thankful to the NIH (CA RO1127369, PO1CA55791), Roswell Park Alliance, the shared resources of the RPCI support grant (P30CA16056) and Photolitec, LLC, E. Amherst, NY.

References

1. Aboul-Enein, H.; Wainer, IW. The impact of stereochemistry on drug development and use, vol. 142 in Chemical Analysis. A series of Monographs on Analytical Chemistry and its applications. Winefordner, JD., editor. New York: John Wiley & Sons, Inc.; 1987.
2. William, IW., editor. Drug Stereochemistry: Analytical Methods and Pharmacology. 2nd ed.. New Work: Marcel Dekker; 1993. and references therein.
3. Wilson K, Walker J. Chirality and its importance in drug development. Biochem. Soc. Trans. 1991; 19:444–475.
4. Rettie AE, Korzekwa KR, Kunze KL, Lawrence RF, Eddy AC, Aoyama T, Gelboin HV, Gonzalez FJ, Trager WF. Chem. Res. Toxicol. 1992; 5:54. [PubMed: 1581537]
5. Knoche B, Blaschke G. Chirality. 1994; 6:221.
6. Portoghese, PS. Handbook of Experimental Pharmacology. Vol. 104. Springer; 1993. Selective Nanopeptide Opioid Anatagonists, Opiods; p. 279
7. Lehmann, FP. Receptors and Recognitions. Curtrecasa, P.; Greaves, MF., editors. Vol. 5. Chapman and Hall; 1978.
8. William K, Lee E. Drugs. 1985; 30:333. [PubMed: 3905334]
9. Ariens EJ. Eur. J. Clin. Pharmacol. 1984; 26:663. [PubMed: 6092093]
10. Simonyi M. Med. Res. Rev. 1984; 4:359. [PubMed: 6087043]

11. Hyneck, M.; Deut, J.; Hook, JB. Chirality in Drug Design and Synthesis. Brown, C., editor. New York: Academic Press; 1990.
12. Tolbert JA, Cirillo VJ, Hitzenberger G, James I, Pryor J, Cook T, Buntinx A, Holmes JB, Lutterbach PM. Clin. Pharmacol. Ther. 1981; 29:144.
13. FDA's policy statement for the development of new stereoisomeric drugs. Chirality. 1992; 4:338. [PubMed: 1354468]
14. Nressler NM. Board Fm Med. 2002; 15:7. and references therein.
15. Richter A, Sternberg E, Waterfield E, Dolphin D, Levy JG. Proc. SPIE Advances in Photochemotherapy. 1997; 1089:132.
16. Pandey RK, Sumlin AB, Potter WR, Bellnier DA, Henderson BW, Constantine S, Aoudia M, Rodgers MR, Smith KM, Dougherty TJ. Photochem. Photobiol. 1996; 63:195.
17. Henderson BW, Bellnier DA, Greco WR, Sharma A, Pandey RK, Vaughan L, Weishaupt KR, Dougherty TJ. Cancer Res. 1997; 57:4000. [PubMed: 9307285]
18. Joshi, P.; Pandey, RK. Synthesis and biological significance of porphyrin-based photosensitizers in photodynamic therapy in Biomedical Photonics Handbook. Vo-Dinh-T, editor. Boca Raton: CRC Press; 2015. p. 31
19. Ethirajan, M.; Patel, NJ.; Pandey, RK. Porphyrin-based multifunctional agents for tumor-imaging and PDT in Handbook of Porphyrin Science. Kadish; Smith; Guilard, editors. Vol. 4. New Jersey: World Scientific; 2010.
20. Pandey, RK.; Zheng, G. Porphyrins as photosensitizers in photodynamic therapy in The Porphyrin Handbook. Kadish, KM.; Smith, KM.; Guilard, R., editors. San Diego: Academic Press; 2000. p. 157
21. Bonnett R. Chem. Soc. Rev. 1995:19.
22. Vogel E, Kocher M, Schmickler H, Lex J. Angew. Chem. 1986; 25:257–258.
23. Blumenkranz MS, Woodburn KW, Qing F, Verdooner S, Kessel D, Miller R. American Journal of Ophthalmology. 2000; 129:353. and references therein. [PubMed: 10704552]
24. Allen CM, Sharman WM, Van Lier JE. J. Porphyrins and Phthalocyanines. 2001; 5:161. and references therein.
25. Wohrle D, Shopova M, Muller S, Milev AD, Mantareva VN, Krastev KK. J. Photochem and Photobiol, B: Biology. 1993; 21:155. and references therein.
26. Ethirajan M, Chen Y, Joshi P, Pandey RK. Chem. Soc. Rev. 2011; 40:340. [PubMed: 20694259]
27. Zhang, S.; Patel, NJ.; Pandey, RK. Chlorophyll-a analogs for cancer-imaging and therapy (Theranostics) in Applications of Porphyrinoides in Alpplications of Porphyrinoides. Paolesse, R., editor. Berlin: Springer-Verlag; 2014. p. 1
28. Pandey, RK.; James, NS.; Chen, Y.; Missert, J.; Sajjad, M. Bifunctional agents for imaging and therapy in Springer Protocols, Photodynamic Therapy, Methods and Protocols. Gomer, C., editor. Springer New York: Humana Press; 2010. p. 223
29. Gupta, A.; Pandey, RK. Supramolecular approach for tumor imaging and photodynamic therapy in Supramolecular Systems in Biomedical Fields. Schneider, H-J., editor. The Royal Society of Chemistry: 2013. p. 451Chapter 15
30. Pandey SK, Gryshuk AL, Sajjad M, Zheng X, Chen Y, Abouzeid MM, Morgan J, Charamisinau I, Nabi HA, Oseroff AR, Pandey RK. J. Med. Chem. 2005; 48:66286.
31. Pandey SK, Sajjad M, Chen Y, Pandey A, Missert JR, Batt C, Yao R, Nabi HA, Oseroff AR, Pandey RK. Bioconjugate Chem. 2009; 52:445.
32. Srivatsan A, Yanfang W, Joshi P, Sajjad M, Chen Y, Liu C, Thankppan K, Missert JR, Tracy E, Morgan J, Rigual N, Baumann H, Pandey RK. J. Med. Chem. 2011; 54:6859. [PubMed: 21842893]
33. Azar, FS.; Intes, X., editors. Translational Multimodality: Optical Imaging. Boston: Artech House; 2008.
34. Yodh, AG.; Konecky, SD. Diffuse optical imaging and PET imaging in Translational Multimodality. Azar; Intes, editors. Boston: Artech House; 2008. and references therein.
35. Curtin L, Sexton B, Pandey RK. Unpublished results.

36. Tracy EC, Bowman H, Pandey RK, Henderson BW, Baumann H. Photochemistry and Photobiology. 2011:1405. [PubMed: 21883244]
37. Smith KM, Goff DA, Simpson DJ. J. Am. Chem. Soc. 1985; 107:4941.
38. Pandey RK, Bellnier DA, Smith KM, Dougherty TJ. Photochem. Photobiol. 1991; 53:65. [PubMed: 2027908]
39. Tamiaki H, Kouraba M, Takeda K, Kondo S-I, Tanikaga R. Tetrahedron Asymmetry. 1998; 9:2101.
40. Courtney S, Baumann H, Pandey RK. Unpublished results.
41. Henderson BW, Daroqui C, Tracy EC, Vaughan LA, Loewen GM, Cooper MT, Baumann H. Clin. Cancer Res. 2007; 13:3156. [PubMed: 17545518]
42. Liu W, Baer MR, Bowman MJ, Pera P, Zheng X, Morgan J, Pandey RK, Oseroff AR. Clin. Cancer Res. 2007; 13:2463. [PubMed: 17438106]
43. Morgan J, Jackson JD, Zheng X, Pandey SK, Pandey RK. Molecular Pharmaceutics. 2010; 7:1789. [PubMed: 20684544]
44. Mettath S, Munson B, Dougherty TJ, Pandey RK. Bioconjugate Chem. 1999; 1:94.
45. Rungta A, Zheng G, Missert JR, Potter WR, Dougherty TJ, Pandey RK. Bioorg. Med. Chem. Lett. 2000; 10:1463. [PubMed: 10888333]
46. Zheng G, Camacho S, Potter W, Bellnier DA, Henderson BW, Dougherty TJ, Pandey RK. J. Med. Chem. 2001; 44:1540. [PubMed: 11334564]
47. Gryshuk A, Chen Y, Goswami LN, Pandey SK, Missert JR, Ohulchanskyy T, Potter W, Prasad PN, Oseroff A, Pandey RK. J. Med. Chem. 2007; 50:1754. [PubMed: 17371002]
48. For advanced fluorescence pre-clinical imaging, the IVIS Spectrum has the capability to use either trans-illumination (from the bottom) or epi-illumination (from the top) to illuminate in vivo fluorescent sources. 3D diffuse fluorescence tomography can be performed to determine source localization and concentration using the combination of structured light and trans illumination fluorescent images. The instrument is equipped with 10 narrow band excitation filters (30nm bandwidth) and 18 narrow band emission filters (20nm bandwidth) that assist in significantly reducing autofluorescence by the spectral scanning of filters and the use of spectral unmixing algorithms. In addition, the spectral unmixing tools allow the researcher to separate signals from multiple fluorescent reporters within the same animal (see: invivoimaging@perkinelmer.com)
49. Angel E, Spetalen S, Madsen SJ, Sun CH, Peng Q, Carper SW, Sioud M, Hirschberg H. J. Neurosurg. 2006; 104:109. [PubMed: 16509154]
50. Tamiaki H, Amakawa M, Tanikaga R, Holzwarth AR, Schaffner K. Photochem. Photobiol. 1996; 63:92–99.
51. Sudlow G, Birkett DJ, Wade DN. Mol. Pharmacol. 1976; 12:1052. [PubMed: 1004490]
52. Chen Y, Miclea R, Srikrishnan T, Balasubramanian S, Dougherty TJ, Pandey RK. Biorg. Med. Chem. Lett. 2005; 15:3169.

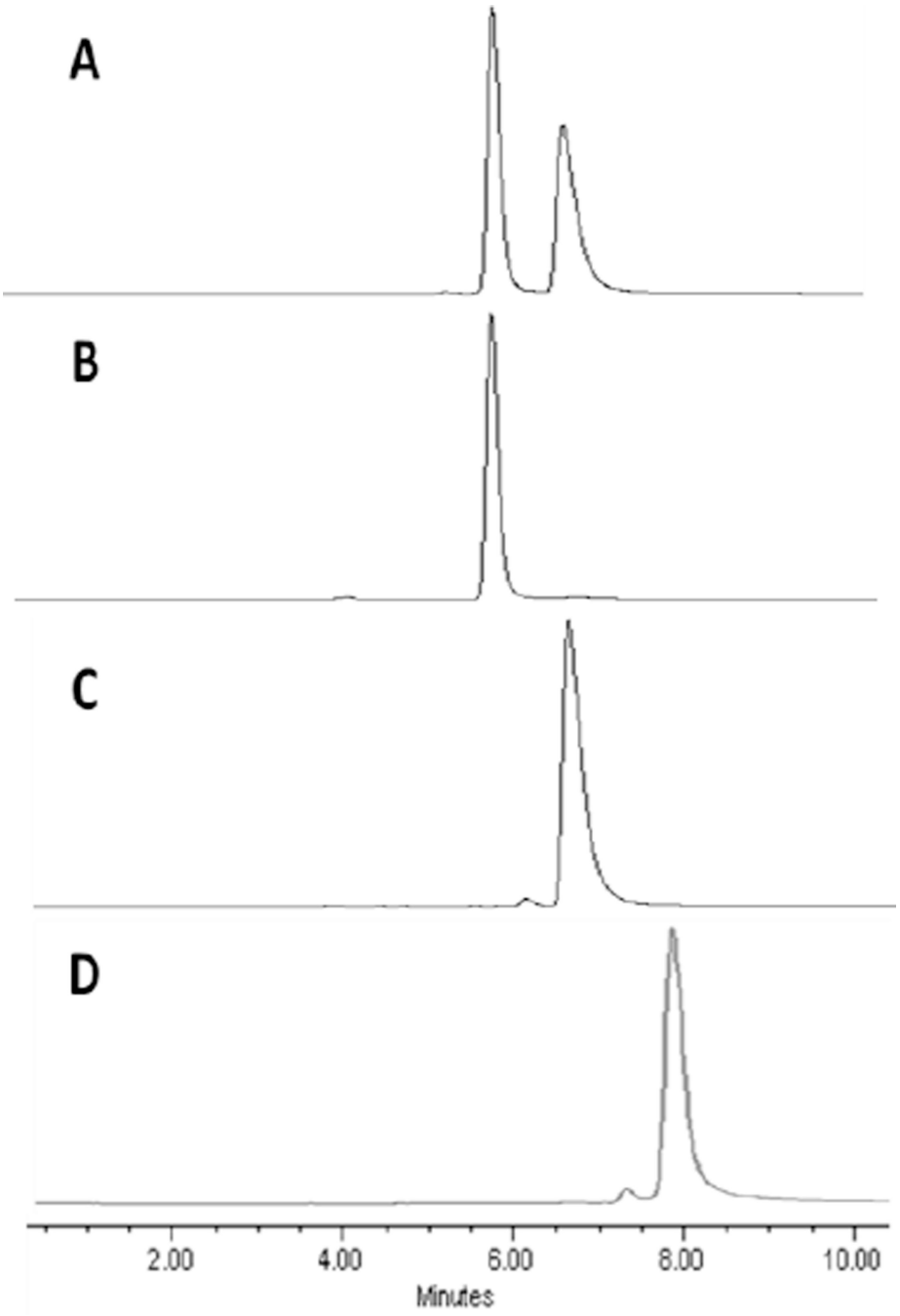

Figure 1.

HPLC was carried out using a Waters Delta 600 system consisting of the 600 Controller, 600 Fluid Handling Unit and 996 Photodiode Array Detector equipped with a Chiralpak IB column with dimensions 4.6 × 250 mm, 5 μm particle size. The mobile phase was isocratic: 40% ethyl acetate–60% hexane at a flow rate of 1.0 ml/min. Chromatographs indicate: A, compound **2**; B, compound **3**; C, compound **4**; and D, compound **9**. The retention times for isomers **3** and **4** were 5.9 and 6.6 min, respectively. The retention time for nonchiral compound **9** was 8.0 min.

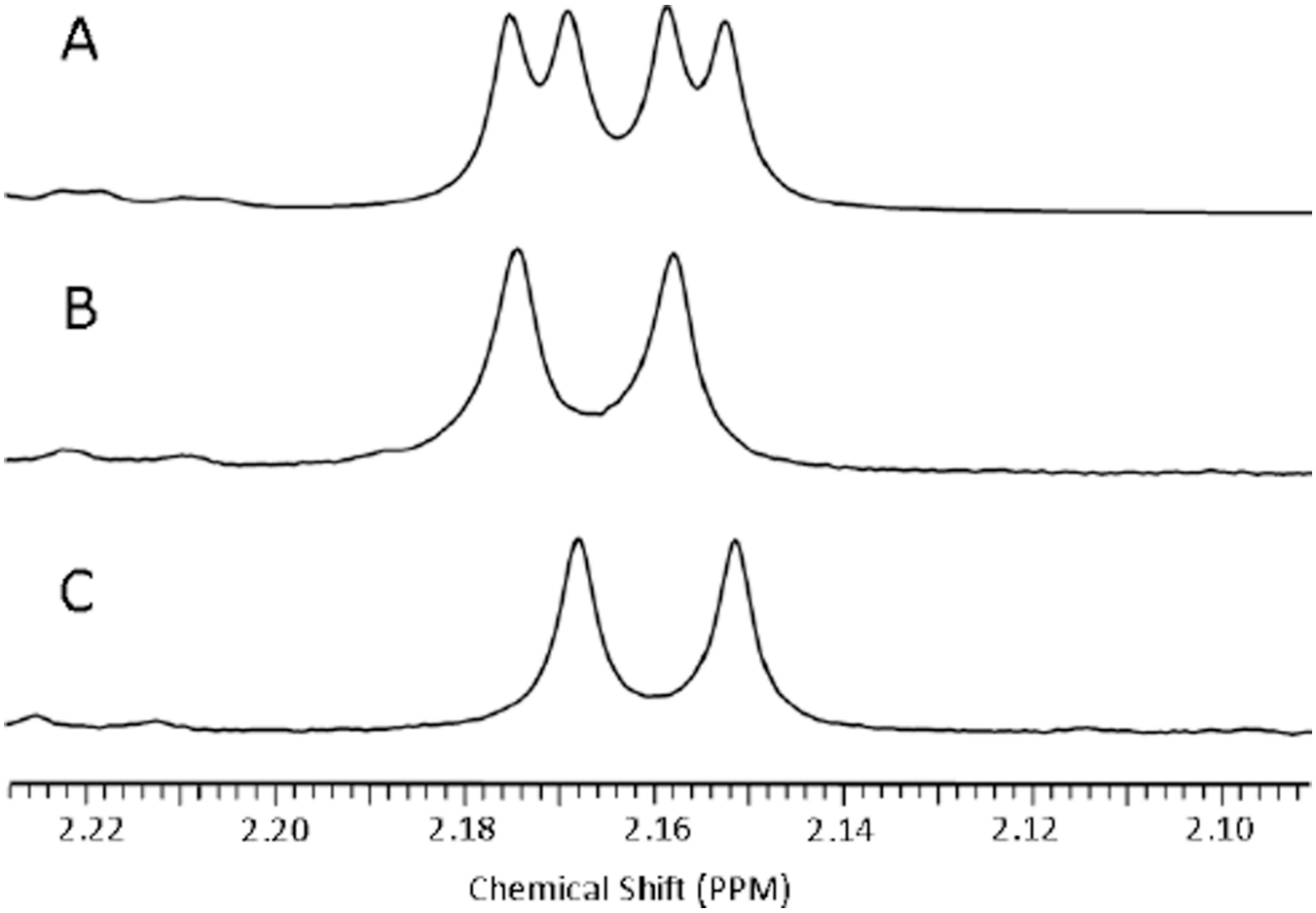

Figure 2.

Partial ^{1}H NMR spectra show slight differences in the chemical shifts of the 3^{1} methyl proton doublets of compound **3** (B) and compound **4** (C). In compound **2** (A) both doublets are present, as expected for the mixture containing both forms. In both (B) and (C), the presence of only one set of peaks suggests that **3** and **4** are isomerically pure.

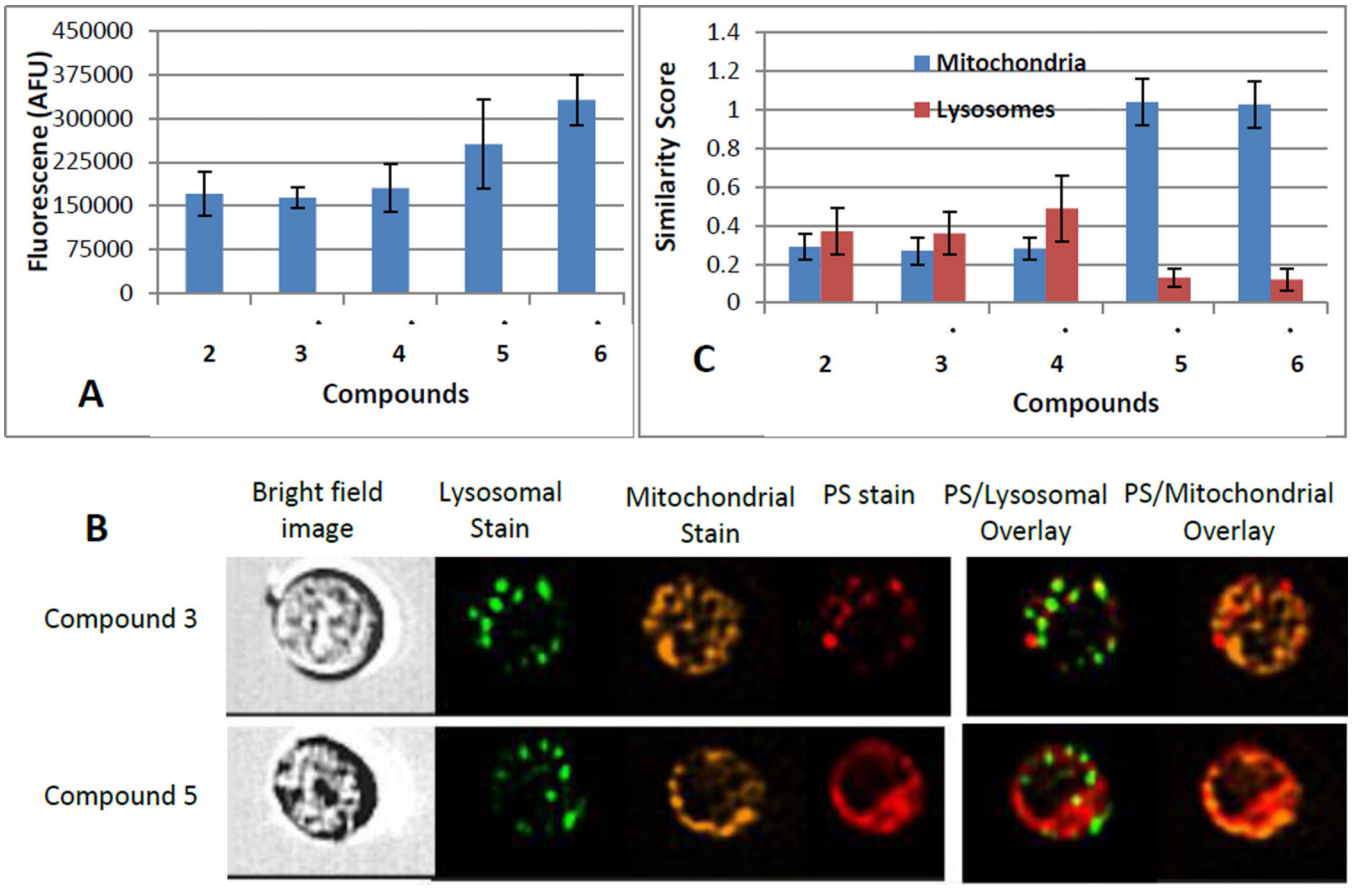

Figure 3.

Uptake and intracellular localization of the compounds 2–6 in colon 26 cells after 24 hour incubation in medium containing 0.8 μM compounds. (**A**): Total intracellular uptake determined by fluorescence. (**B**): Representative images from flow cytometry analysis (Image Stream) comparing subcellular distribution of compounds and organelle-tracking dyes. (**C**): Similarity Score as a measure for co-localization of the compounds with the lysosomal and mitochondrial markers (the higher positive the score the more closely the fluorescent probes co-localize). Data represent the means ±SD of replicate samples from 3 separate experiments).

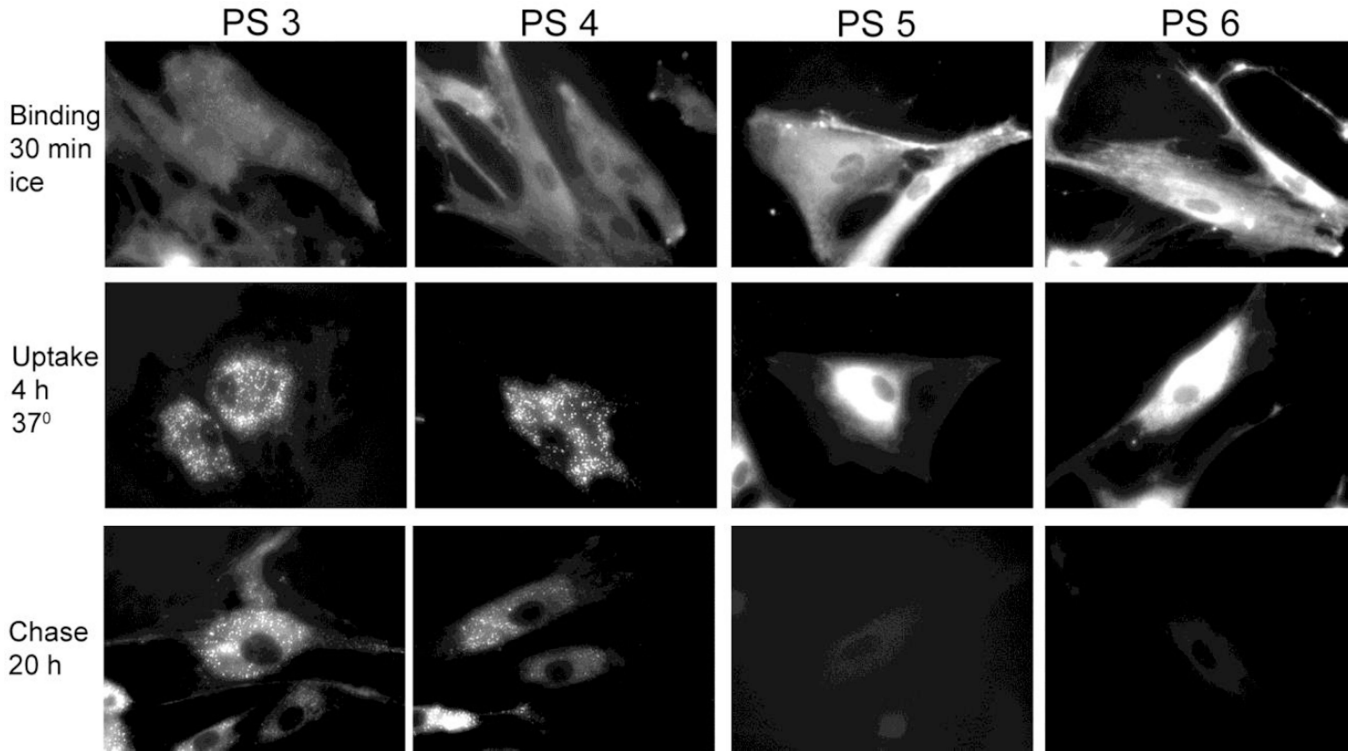

Figure 4.

Binding and intracellular retention of compounds **3–6** (*PS 3–6*) by human lung tumor fibroblasts. Subconfluent cultures of fibroblast were incubated in medium containing 3.2 μM of the indicated compunds. Binding to the cells was determined by 30-min exposure at 0°, uptake by incubation of the cells for 4 hours at 37° and retention by culturing in compound-free medium for 20 hours. Cell-associatied fluorescence of the compounds was visualized by microscopy (400× magnification).

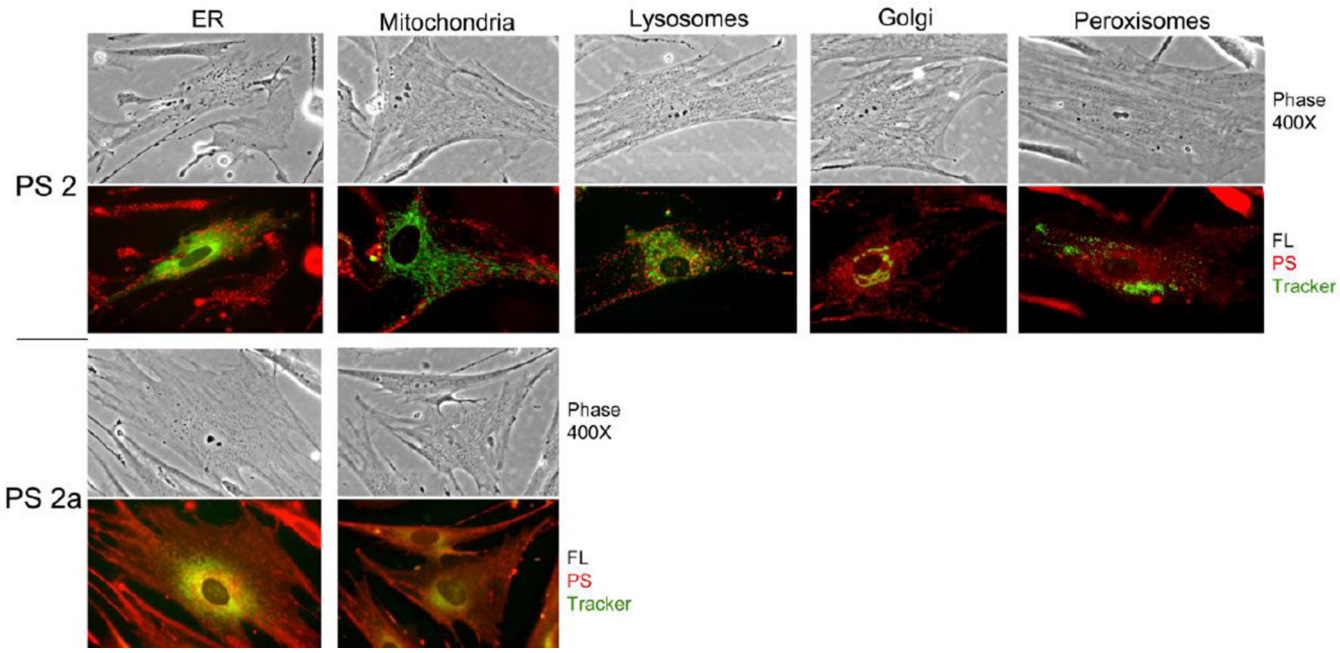

Figure 5.

Subcellular localization of compounds 2 and 2a in lung tumor fibroblasts. Primary cultures of tumor-derived fibroblasts were transduced with vectors encoding ER-GFP, Golgi-GFP or Peroxisome-RFP. After 24 h, the cells were incubated for 4 hours with compound **2** or compound **2a**. Thirty min prior to the end of incubation, separate cultures were stained with Mito-tracker green or Lysotracker green. All cultures were analyzed by phase contrast and fluorescent microcopy at 400×. All organelle markers are colorized in green, and fluorescence for compounds **2** and **2a** is shown in red.

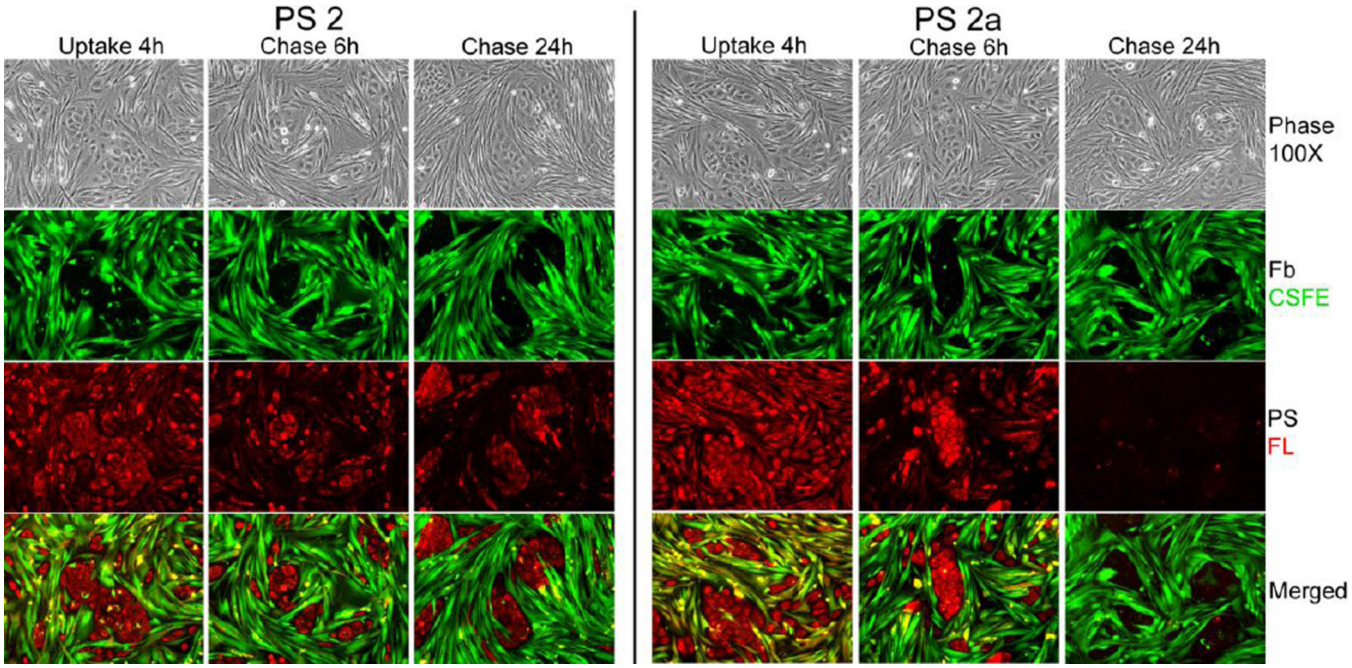

Figure 6.

Lung tumor cell-specific retention of compounds 2 and 2a (PS 2 and PS 2a). Co-cultures of primary lung squamous carcinoma cells and CSFE-labeled stromal fibroblasts were incubated for 4 h with culture medium containing 3.2 μM PS 2 or PS 2a followed by 6 and 24 h chase in PS-free medium. The culture-associated fluorescence was recorded at the times indicated by microscopy.

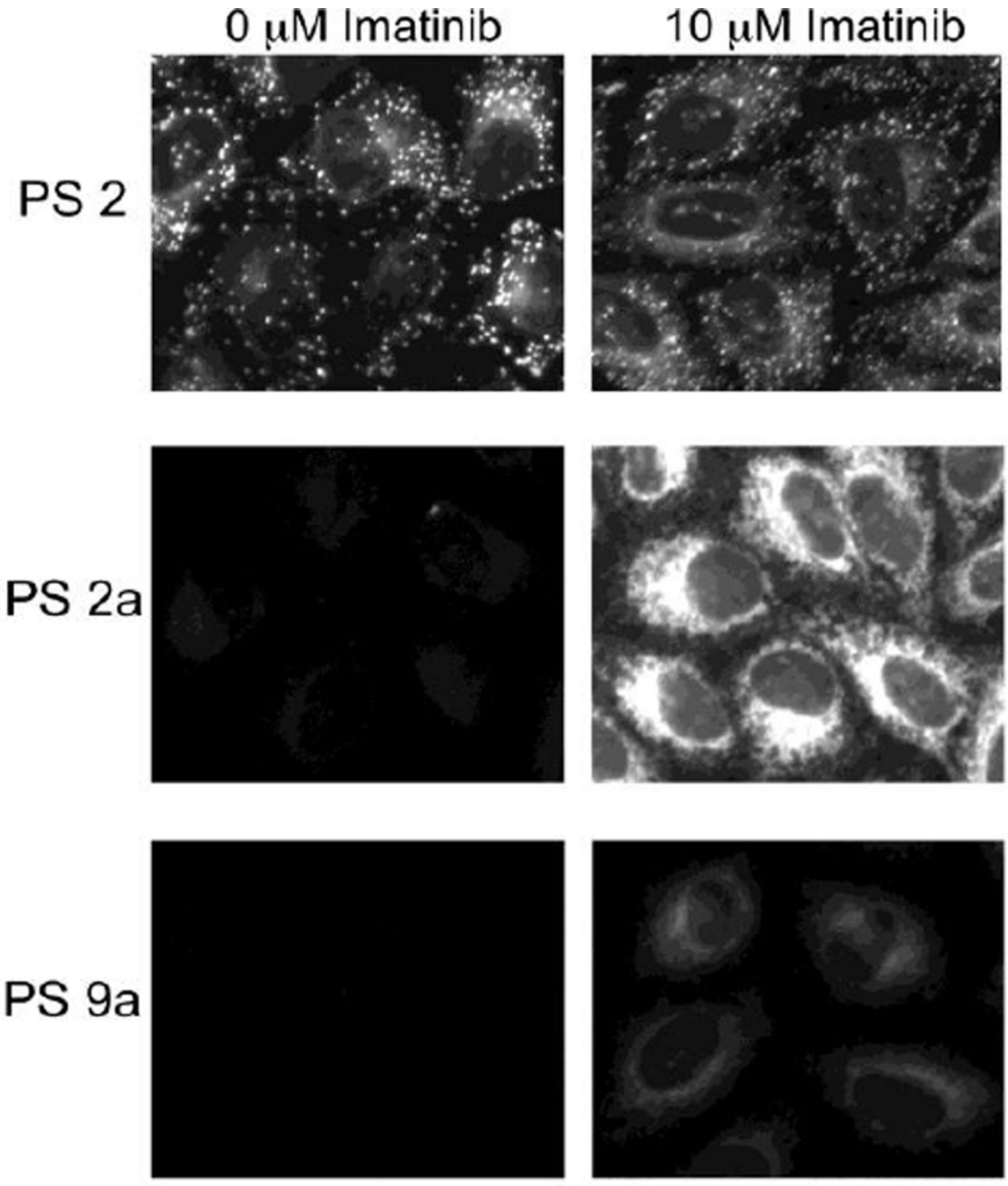

Figure 7.

Cellular export of carboxylic acid derivatives controled by ABCG2. Primary cultures of ABCG2-positive L352 epithelial cells were incubated for 30 min at 37° in serum-free medium containing 3.2 μM compounds **2** (PS 2), **2a** (PS 2a) or **9a** (PS 9a). The cells were washed and incubated for 4 hours in compound-free medium containing 10% FBS and either 0 or 10 μM imatinib mesylate. Cell-associated compounds were determined by fluorescence microscopy at 400× magnification using identical camera setting.

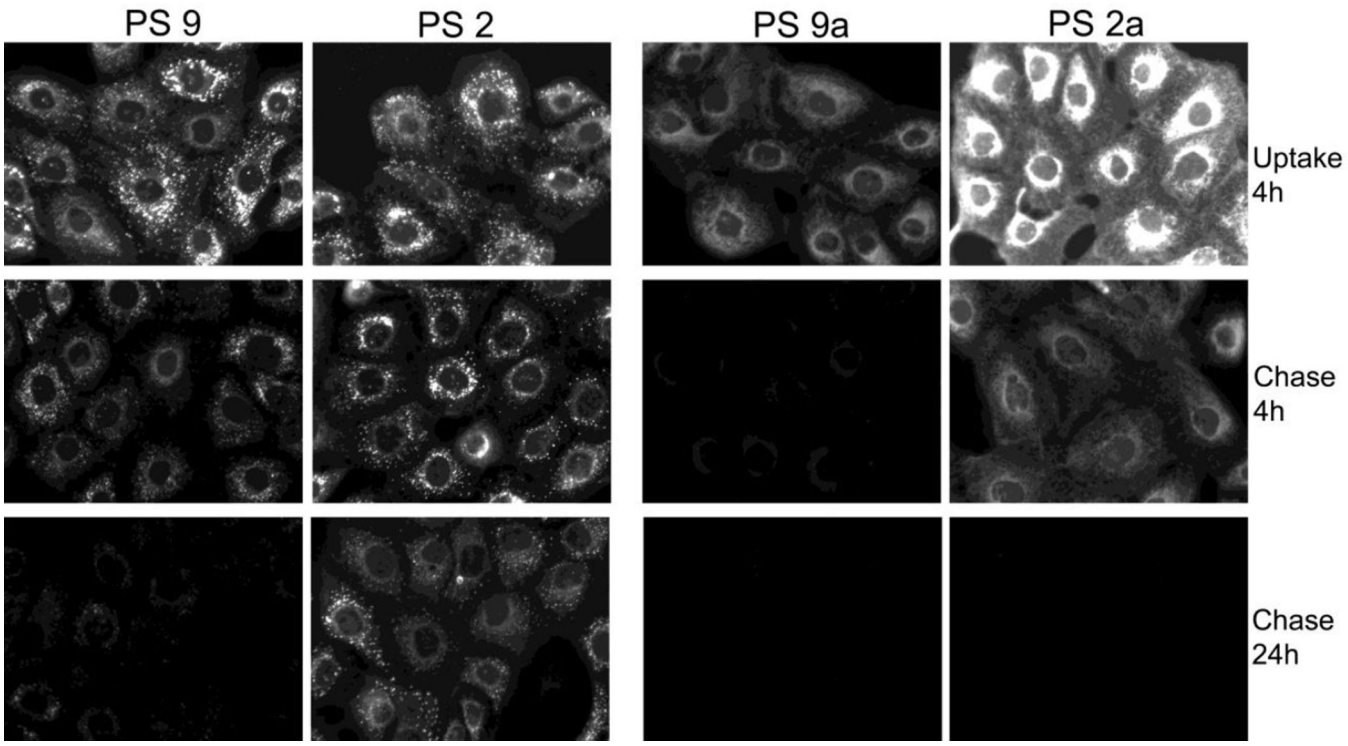

Figure 8.

Effect of the 3'-chiral center on cellular retention in lung tumor cells. Replicate 6-well culture plates of lung tumor epithelial cells were incubated for 4 h in culture medium containing 10% FBS and 800 nM of PS **2, 2a** or non-chiral PS (**9** and **9a**). The cells were washed free of PS and imaged at 400× magnification under fluorescence. Cells were incubated in PS-free medium containing 10% FBS for additional 4 and 24 hours.

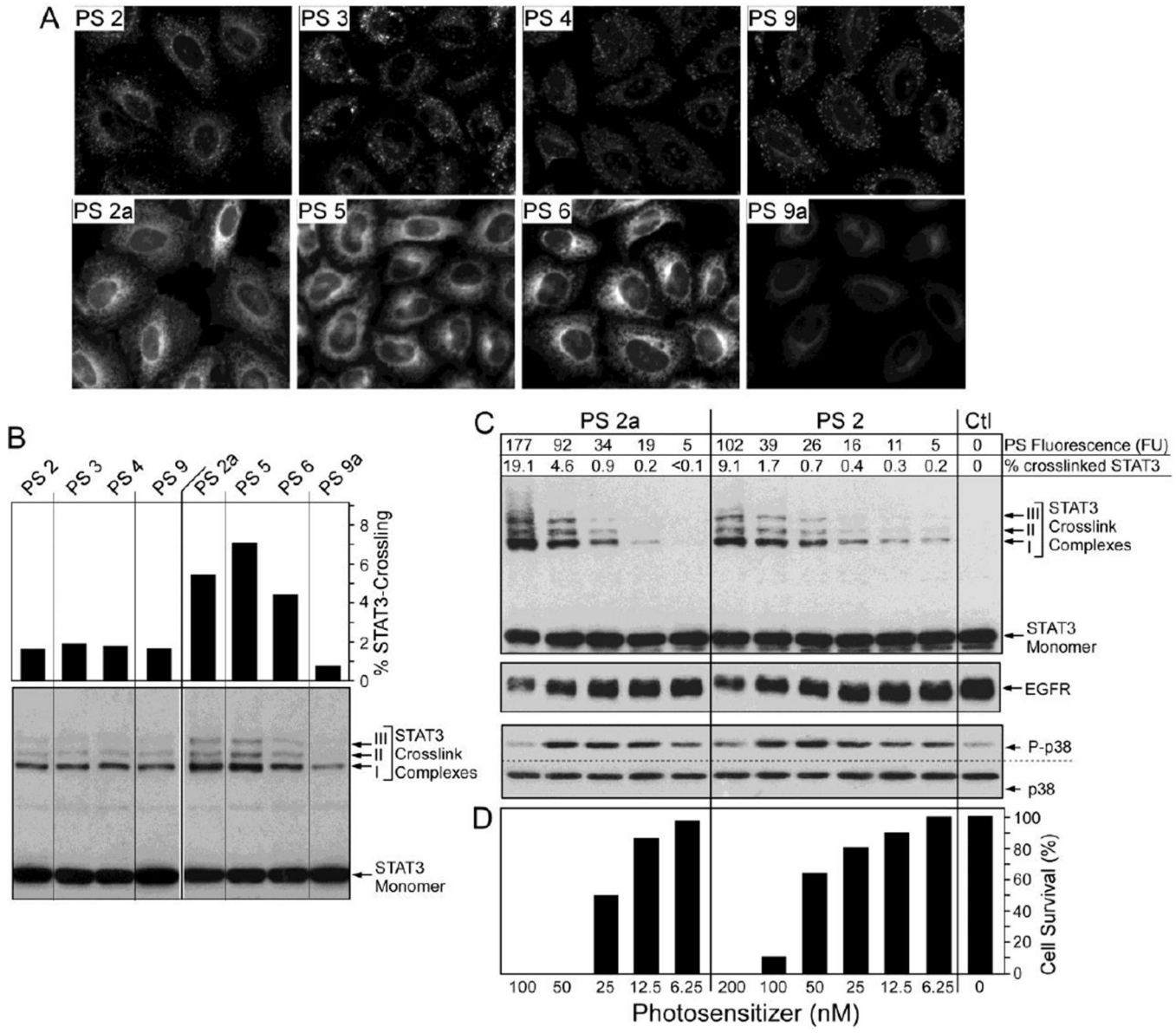

Figure 9.

Correlation of compound uptake and photoreaction. Confluent epithelial cells were incubated for 4 hours with 800 nM (for fluorescent imaging in A) or 100 nM (for biochemical analysis in B–D) compounds listed at the top. After a 4-h chase period, the cell-associated fluorescence was determined by imaging. The cells in B–D were treated with 665nm light (3 J/cm^2), extracted and the relative amount of oxidative crosslinking of STAT3 and level of EGFR and phospho- and total p38 MAPK were determined by immunoblotting.

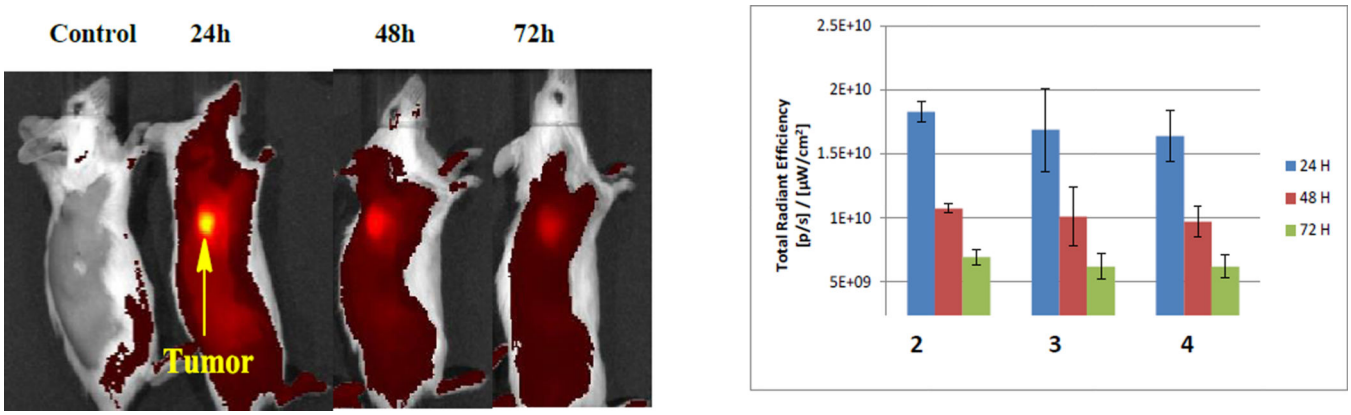

Figure 10.

In vivo fluorescence detection of compound PS 2 and its isomers 3 and 4 accumulation in the colon26 tumors. Representative Images of 1 μmole/kg PS 2 injected i.v. and imaged at 24, 48 and 72 hours post injection (excitation wavelength - 675 nm, emission wavelength −720 nm). B: Data represent the mean fluorescence expressed as total radiant efficiency ±SD of 3 mice/group.

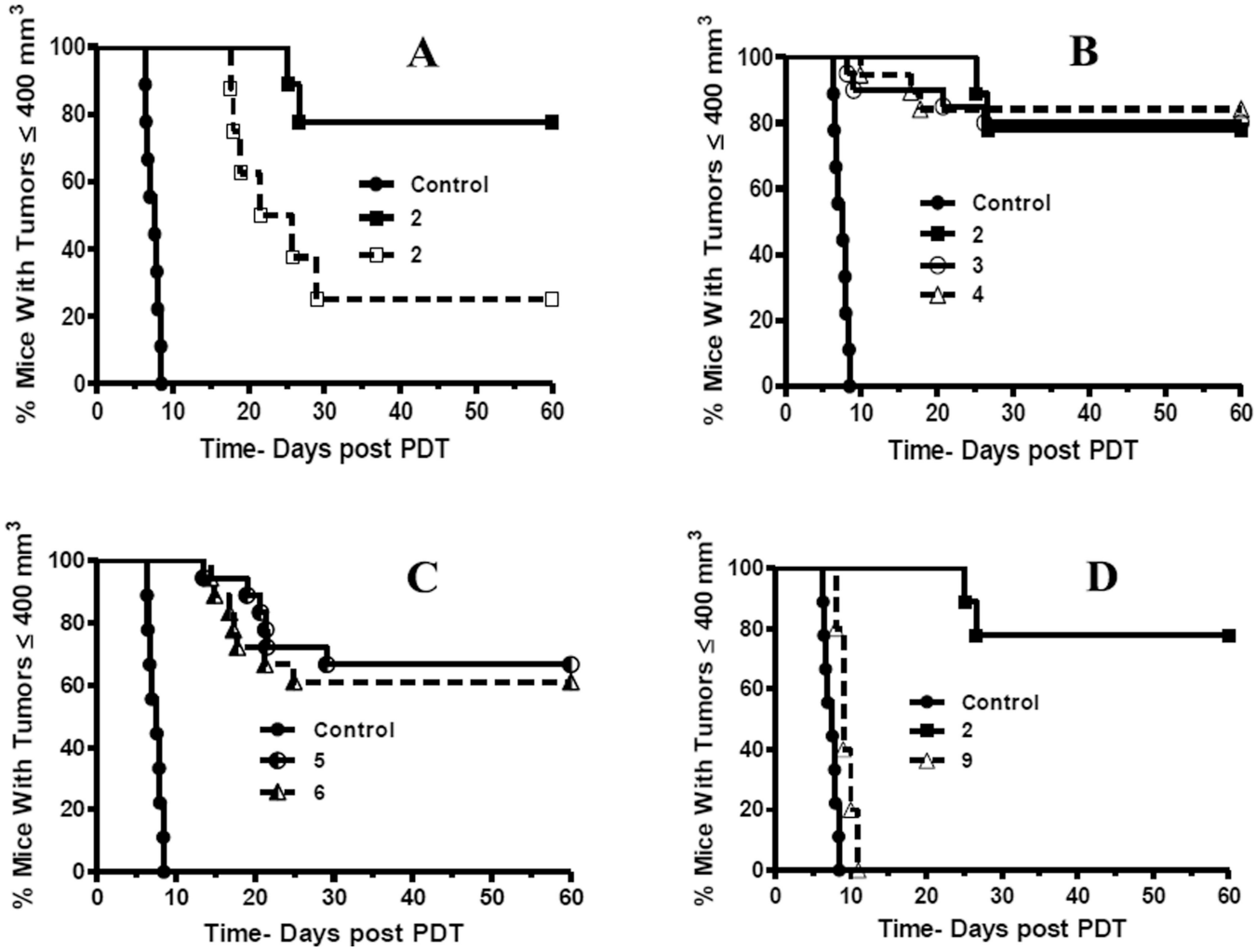

Figure 11.

Comparative *in vivo* photosensitizing efficacy of PSs in BALB/c mice bearing Colon 26 tumors at variable light doses. In four separate sets of experiments, tumor-bearing mice were subjected to following treatments: all PS injections were i.v. at 1.00 μmol/kg with light treatment of the tumor 24 h later. (A): PS 2 (with laser light at 665 nm using two conditions: 135 J/cm^2, 75mW/cm^2 (-▭-) and 128J/cm^2, 14 mW/cm^2, (—■—)]. (B): PS 2 and the corresponding *R*- and S- isomers 3, 4; (C): isomers 5 and 6 and, (D): PS 2 and PS. 9 (achiral at position-3). All animals in B to D were treated with 665 nm light (128J/cm^2, 14 mW/cm^2), Tumor growth was monitored daily for 60 days.

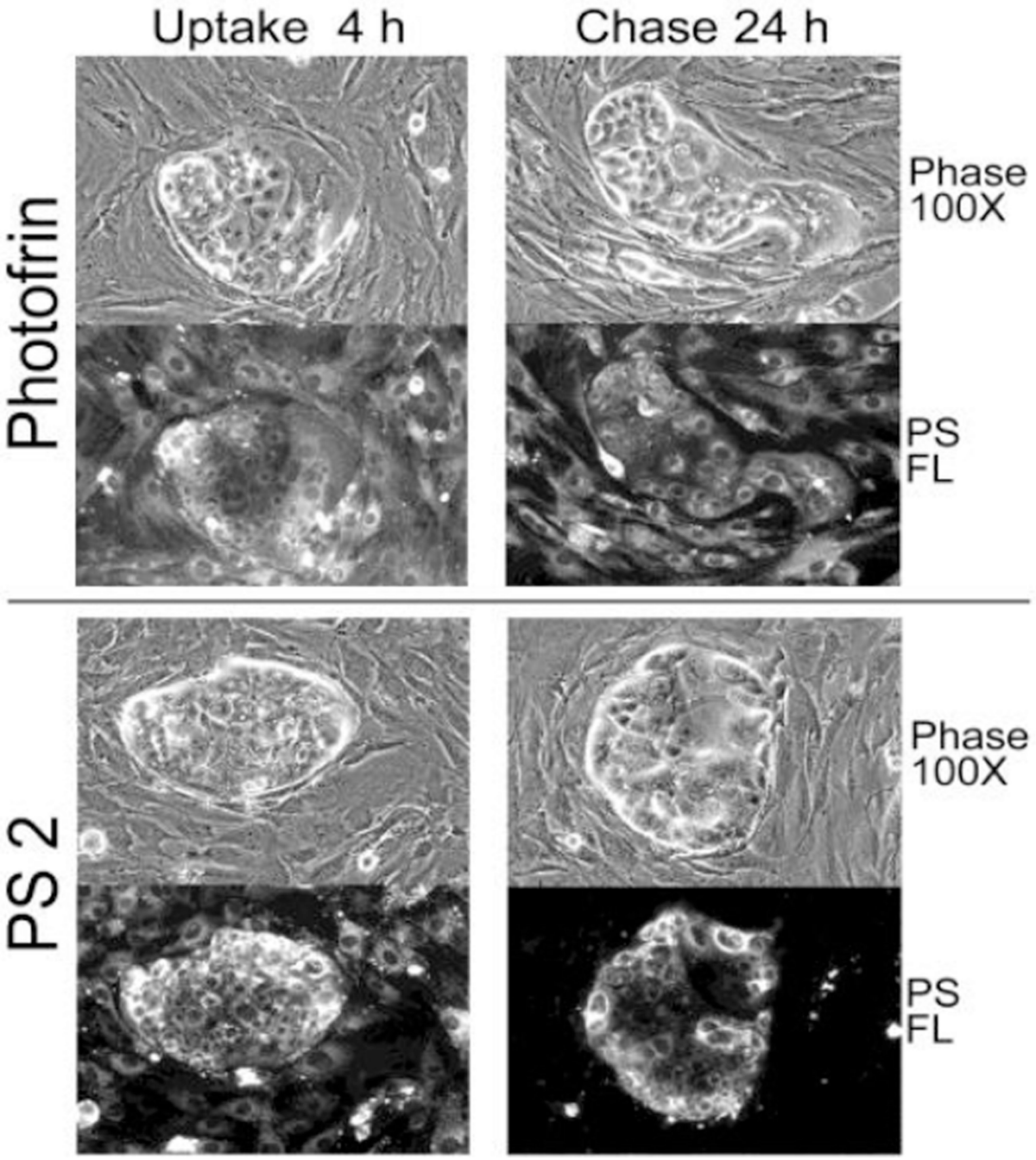

Figure 12.

PDT efficacy of Compound 2 (PS2) and Photofrin (PFII) on human NSCLC xenograft tissue. Xenograft tissue was dissociated, plated onto collagen-1 matrix and cultured for 4 days. The tumor cells form clusters segregated from stromal cells. The cultures were treated for 4 hours with medium containing 6μg/ml **PFII** or 1μg/ml PS **2**. The cell-associated PS fluorescence was recorded immediately after uptake and after a 24-hour chase period. The phase microscopic and corresponding fluorescent images at 100× are reproduced.

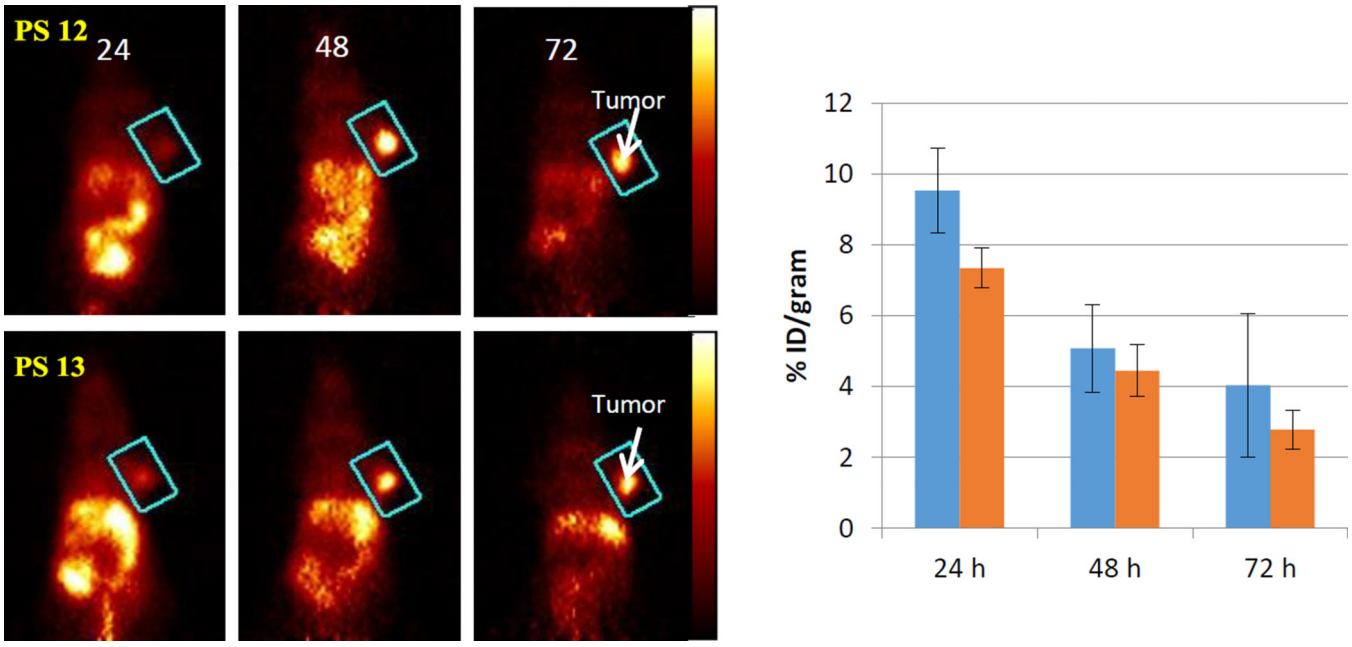

Figure 13.

Coronal view PET images of a BALB/c mouse bearing Colon26 tumor on the right shoulder with labeled ^{124}I-PS 12 or 13 (50μCi). The images were acquired for 30 min at 24, 48, and 72 hours post-injection. The tumor was identified to be within the region defined by a cylinder indicated by the blue rectangle in each image. The color palette (shown on the right) for each image shown was scaled to the min/max of each data set. The tumor uptake (3 mice/group) of the isomers at various time points (24, 48 and 72 hours) is represented in bar graph and shows similar pattern of uptake and clearance. The absolute tumor-uptake was higher at 24 hours post-injection, but tumor contrast was better at 48 and 72 hours post-injection, which could be due to faster clearance of the compounds from other organs than tumor.

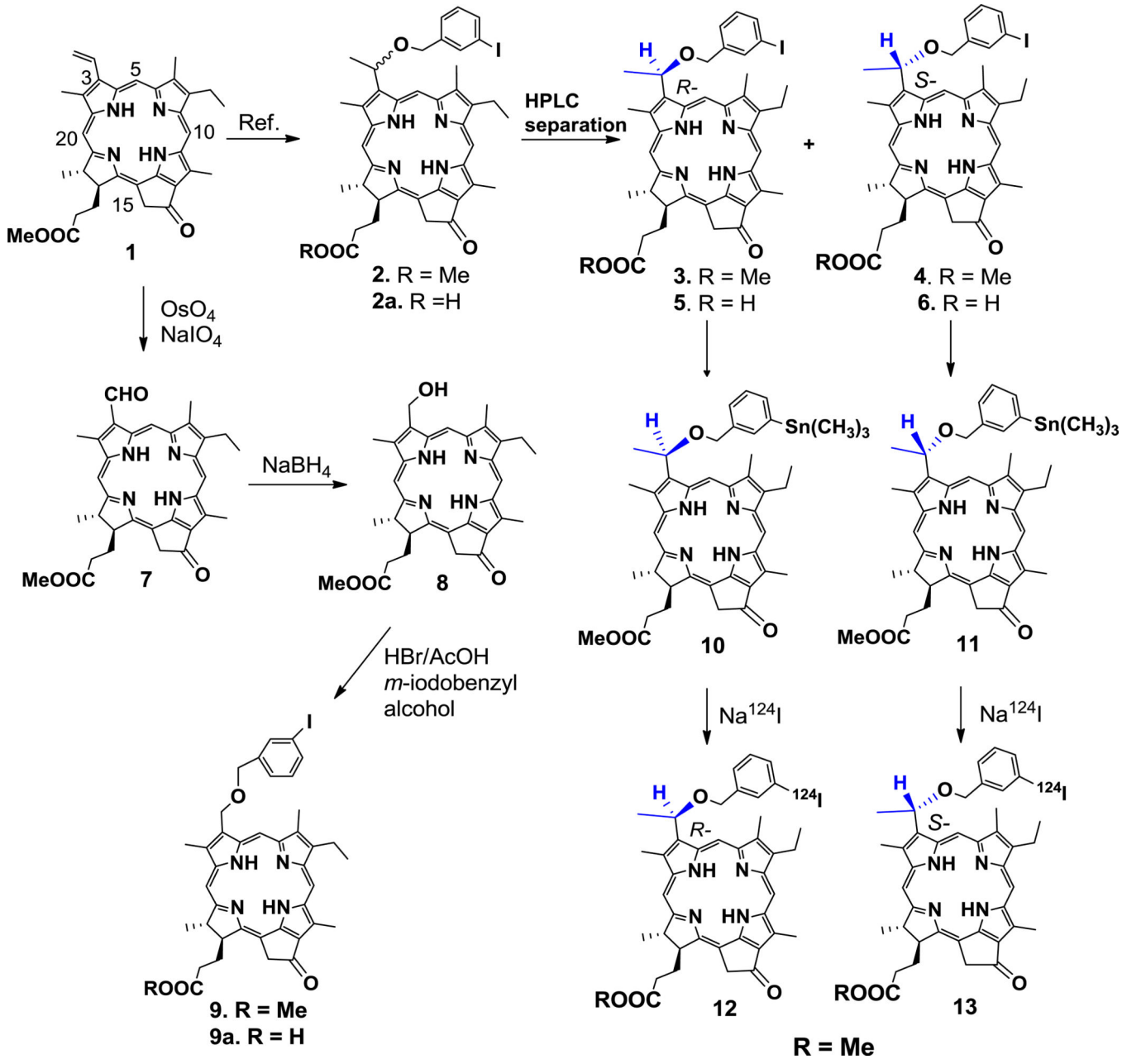

Scheme 1.

Synthesis of iodinated photosensitizers with and without the presence of a chiral center at position-3.